

1

Introduction

“To see a World in a Grain of Sand” (William Blake) [1] – “not only one world and not only in a grain of sand,” a researcher working in the field of super-resolution microscopy might comment. Advanced far-field light-optical methods have become an indispensable tool in the analysis of nanostructures with applications both in the field of material sciences and in the life sciences. Tremendous progress has been made in recent years in the development and application of novel super-resolution fluorescence microscopy (SRM) techniques. As a joint effort by researchers in multiple disciplines, including chemistry, computer sciences, engineering, and optics, the development of SRM has its own place in the long history of light-optical microscopy, culminating in the 2014 Nobel Prize in Chemistry being awarded to Eric Betzig, Stefan Hell, and William E. Moerner for their achievements in the advancement of single-molecule detection and super-resolution imaging [2]. More precisely, these researchers succeeded in developing revolutionary new microscopy techniques that can be used, for example, in the investigation of fluorescent cell samples down to the level of individual molecules, that is, they cleared the way for new approaches that have proven invaluable for a wide range of applications in biomedical research. This is due to the fact that after specific labeling of a target structure with fluorescent markers, a fluorescence readout can be analyzed with respect to its spatial and temporal distribution, and thus it provides great detail about the underlying structure [3]. As the background in fluorescence imaging is typically close to zero, the resulting contrast allowed even the detection of single molecules [4]. Despite these developments, none of the novel SRM techniques has so far invalidated Abbe’s (1873) or Rayleigh’s (1896) limits for the resolution of light-optical microscopy; methods of circumventing these limitations have been discovered. By implementing these methods it became possible for the first time to, for example, directly observe the molecular machinery of life by far-field light microscopy.

This introduction presents the basic physical concepts behind the limits in optical resolution and offers an up-to-date diachronic overview of some important landmarks in the development of SRM methods. The next two chapters focus on the physicochemical background (Chapter 2) and required hardware and software (Chapter 3). The next four topic-specific chapters are dedicated to a description and evaluation of structured illumination microscopy (SIM) (Chap-

ter 4), localization microscopy, and in particular single-molecule localization microscopy (SMLM) (Chapter 5), stimulated emission depletion (STED) microscopy (Chapter 6), and multi-scale imaging with a focus on light-sheet fluorescence microscopy (LSFM) and optical projection tomography (OPT), as well as on sample preparation techniques such as clearing and expansion microscopy (ExM) (Chapter 7). These application-oriented chapters are not restricted to a mere description of the respective techniques but offer a thorough discussion and evaluation of the specific potentials and problems of the various methods. Each of these advanced light-optical microscopy techniques responds in its own specific way to the research question and challenges at hand, and each of them comes with its own set of benefits and disadvantages. The discussion (Chapter 8) finally tries to push the limits by shedding light on potentially promising progressive approaches and future challenges in this ever-growing and extremely fast developing field. A particular focus in all of the discussions will be on the application of advanced light-optical microscopy in studies of biological cell samples.

In the visible range of the electromagnetic spectrum, cells can be considered thick, transparent objects that can be analyzed in three dimensions by means of far-field light microscopy either after fixation in a preserved state or possibly as live samples. However, the images produced by this analysis method lack structural information owing to the limited resolution of light microscopy. In recent years, a number of methods of fluorescence microscopy have been developed to narrow down the spread of the blur in microscopic images or to facilitate the separate detection (localization) of individual fluorescent molecules within samples and, thus, to prevent the “Abbe limit of microscopic resolution” from being applicable to the final microscopic image, resulting in the transition from microscopy to nanoscopy. The realization of focused nanoscopy-based STED and localization microscopy-based photoactivated localization microscopy (PALM) techniques represents culminating points of a long history of attempts to overcome the so-called Abbe limit: In 1873, Ernst Abbe, the colleague of Carl Zeiss, in his pioneering developments of advanced microscopy, stated that “[...] the limit of discrimination will never pass significantly beyond half the wavelength of blue light [...],” which corresponds to approximately 200 nm. A similar limit for the possibility to distinguish two “point-like” luminous objects was given by Lord Rayleigh in 1896. Point-like means that the dimensions are much smaller than the wavelength used for imaging. From this time on, for about a century, the 200 nm value of the Abbe limit has generally been regarded as the absolute limit for obtaining structural information by far-field light microscopy. However, already in his famous contribution (1873) on the fundamental limits of optical resolution achievable in (far-field) light microscopy, Abbe stated that the resolution limit of about half the wavelength used for imaging is valid only “[...] so lange nicht Momente geltend gemacht werden, die ganz außerhalb der Tragweite der aufgestellten Theorie liegen [...]”¹⁾ As seemingly foreseen by Abbe, only by deviating from

1) Which translates as “[...] as long as no different conditions are introduced that are completely beyond the theory stated here [...]” [UB].

the experimental conditions stated in his original work could super-resolution by STED and PALM be achieved.

1.1

Classical Resolution Limit

In 1873, Ernst Abbe derived from theoretical considerations a criterion for the resolution limit of a light microscope. The considerations that led to its formulation are as brilliant as they are simple: He understood that an object consisting of small structural features gives rise to diffraction, which is known to be stronger for smaller structures. The plethora of structural features present in a real object might be approximated locally by a superposition of stripes of different orientations, stripe widths, and strengths. This will help us in what follows to understand the concepts behind the image blur. Let us consider a fine grating structure with lattice constant d (spacing between two stripes), embedded in a medium with refractive index n , which is *illuminated centrally* with light of wavelength λ/n (λ being the vacuum wavelength). This will result in constructive interference of order m observed under an angle α if the following condition is fulfilled:

$$\frac{m\lambda}{n} = d \sin(\alpha). \quad (1.1)$$

When imaged by a lens, such an interference pattern will only be transmitted under the condition that, in addition to the central non-diffracted beam, at least the $m = \pm 1$ orders are collected by the lens, i.e., two fine object features have a minimum distance $d_{\text{centr.illum.}} = \lambda/(n \sin(\alpha))$. If oblique illumination is used, the minimum distance d for which diffraction arising from the structure is collected by the lens is half the value of $d_{\text{centr.illum.}}$. From this Abbe derived his famous formula for the resolution limit in optical microscopy [5]:

$$d = \frac{\lambda}{2 n \sin(\alpha)}, \quad (1.2)$$

which describes the minimum distance d of two structural features to be resolved by the microscope, where $n \sin(\alpha)$ is the numerical aperture of the detection objective lens, n is the refractive index of the sample, and α is half of the opening angle defined by the rays of light that are detected by the objective lens (acceptance cone); α is the so-called half-aperture angle of the objective lens.

In general terms, Abbe stated a formula for the smallest distance d that two point-like object details can have so that they can still be discriminated (resolved) by microscopy. According to his formula (1.2), the smallest distance d is determined by the vacuum wavelength λ of the light used for imaging and the numerical aperture $n \sin(\alpha)$. For a perfect lens with no spherical aberration, the intensity of the *2D diffraction pattern* of such a single “point source” in the (perfect) focal plane is shown in Figure 1.1a. This diffraction pattern is described [6]

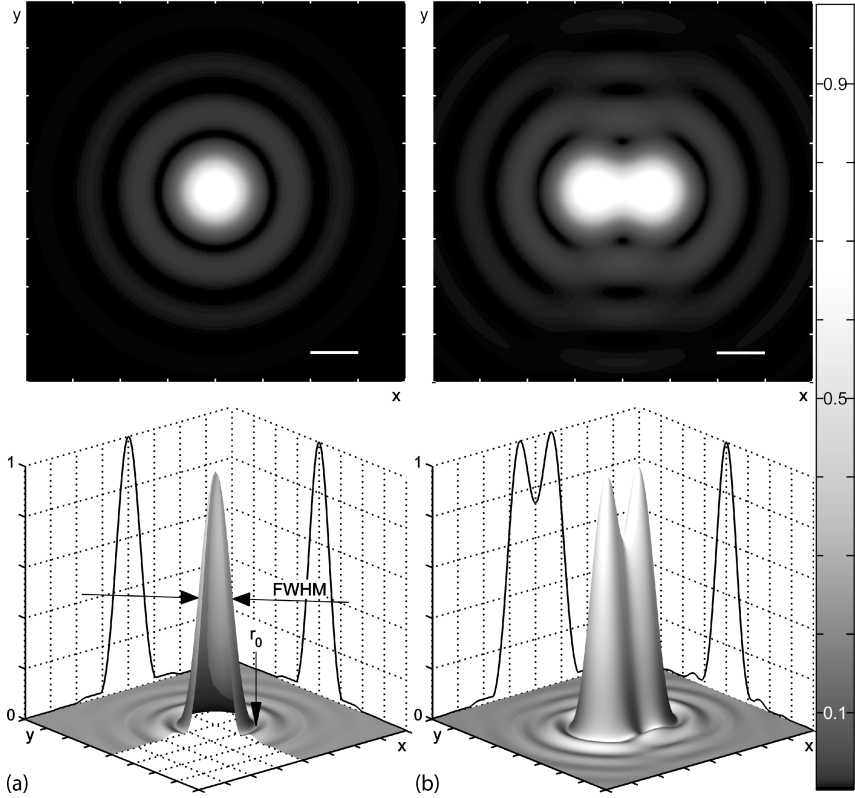


Figure 1.1 Microscopic image of a “point source” (a) or two “point sources” in close proximity (b). Scale bar equals full width at half-maximum (FWHM) of the diffraction pattern of a single “point source.” See text for numeric values.

by the formula

$$I(v) = I_0 \left(\frac{2J_1(v)}{v} \right)^2, \quad (1.3)$$

where J_1 is the first-order Bessel function of the first kind, and v is the (generalized) lateral optical coordinate, related to the image coordinate $r = \sqrt{x^2 + y^2}$ by

$$v(r) = r \frac{2\pi}{\lambda} n \sin(\alpha) = r \frac{2\pi}{\lambda} \text{NA}. \quad (1.4)$$

Knowing the lateral magnification of the microscope system, the image coordinate r can easily be transferred to the object coordinate space, i.e., the coordinates within the sample.

The diffraction pattern in the axial direction is responsible for having point-like objects imaged as elongated structures. The distribution of the diffraction pattern

in the axial direction differs from that in the lateral direction (Equation 1.3). It can be derived [7] (in good approximation) as

$$I_{\text{axial}}(u) = I_0 \operatorname{sinc}\left(\frac{u}{4}\right)^2, \quad (1.5)$$

where $\operatorname{sinc}(z) := \sin(z)/z$, and u is the generalized axial optical coordinate, which depends on the z -displacement $\delta = z' - f$, i.e., on the distance to the ideal (paraxial) focal plane, as follows:

$$\begin{aligned} u &= \frac{2\pi}{\lambda} \frac{\text{NA}^2}{n} (z' - f) \\ &= \frac{2\pi}{\lambda} \frac{\text{NA}^2}{n} \delta. \end{aligned} \quad (1.6)$$

In 1896, Lord Rayleigh put forward his formula for the resolution of an optical instrument, in particular of a light microscope [8], yielding values for the resolution very similar to those obtained by Ernst Abbe. His starting point was the analytical solution of the diffraction pattern of two such “point sources” (Figure 1.1b). By his reasoning, the two sources may be “resolved” if the second source is located at a distance equal to or larger than r_0 , the first minimum of the diffraction pattern of the first source. The position of the first minimum r_0 of Equation 1.3 is given by the first root of the Bessel function $J_1(\nu)$: As a numerical approximation we obtain $\nu(r_0) = 3.83$, or $r_0 = 0.61\lambda/\text{NA}$. The central maximum up to the radius r_0 is called an *Airy disk* of the diffraction pattern. For two objects to be resolved according to the Rayleigh criterion, they must have a minimum distance of

$$d_{\min} = r_0 = 0.61 \frac{\lambda}{n \sin(\alpha)} = 0.61 \frac{\lambda}{\text{NA}}. \quad (1.7)$$

In the simulations shown in Figure 1.1, however, the signals are placed 1 FWHM apart of the diffraction pattern of a single “point source.” The relation between FWHM and d_{\min} is as follows [6]:

$$\text{FWHM} = \frac{0.51}{1.22} \text{AU}, \quad (1.8)$$

where AU is the typical unit used in microscopy called an Airy unit ($1 \text{ AU} = 2 r_0$), indicating the diameter of the Airy disk. For practical reasons, instead of using d_{\min} , which is difficult to measure in noisy data, often the FWHM is used as a resolution criterion, though it is somewhat smaller in value than the resolution limit stated by Lord Rayleigh. As can be seen from Figure 1.1, two objects placed at a distance of 1 FWHM can still be resolved in the absence of noise. Of course, both equations for the resolution (Equations 1.2 and 1.7) are idealized because they do not take, for example, pixelation into account (see also Section 3.2.1 on the localization of emitters).

The derivation of the optical resolution according to Abbe makes use of scattering as a contrast within the sample. Scattering occurs for both coherent and incoherent illumination. Resolution in the transmission microscope, however, is

different for coherent and for incoherent illumination [7]. In the case of fluorescence, the light emitted by different fluorophores is generally considered to be incoherent because of the typical fluorescence lifetimes, which are in the nanosecond range.

The intensity distribution described by Equation 1.3 is normalized to a peak intensity of 1. If instead it is normalized such that the area under the curve is equal to 1, it describes the probability of detecting a photon emitted by the “point source” at $\nu \, d\nu$, and similarly for the axial direction. For this reason, the distributions given by Equations 1.3 and 1.5 (using appropriate normalization) are also called the *point spread function* (PSF) in optical imaging. In signal processing, this corresponds to the impulse response function.

In many practical applications, for example in localization microscopy, it is of interest to measure the peak position of this diffraction pattern, which in the absence of noise and with infinitesimal sampling would be given by the spread of this distribution, as calculated by

$$\sigma_{\text{PSF}} = \int_{-\infty}^{\infty} \nu^2 I(\nu) \, d\nu. \quad (1.9)$$

Paraxial approximation was used in the derivation of Equation 1.3. Nevertheless, the integral $\int_{-\infty}^{\infty} I(\nu) \, d\nu$ is finite. However, using the same derivation and approximations, Equation 1.9 does not converge. A practical way to deal with this – which in fact is used in most applications – is to restrict the evaluation to the central maximum. This is well justified: The central maximum (Airy disk) contributes by approximately 84% to the overall focal-plane intensity, independently of the numerical values for wavelength and NA. Consequently, for most practical implementations, instead of the analytical expression of the intensity distribution inside the Airy disk (Equation 1.3), a Gaussian approximation is used. This substitution using a Gaussian probability distribution has an effect on the accuracy when determining the peak position, which will be discussed in Section 3.2. More recently, especially in three-dimensional (3D) applications, cubic splines have been employed to better approximate the shape of the experimental PSF [9].

Using the PSF to describe the effect of diffraction on a “point source,” the imaging process can be represented by

$$g(\vec{r}) = \int_{-\infty}^{\infty} f(\vec{r}') \text{PSF}(\vec{r}, \vec{r}') \, d\vec{r}', \quad (1.10)$$

where \vec{r}, \vec{r}' are 3D position coordinates, g is the image, f is the object. If the PSF is the same for every position in the sample and depends linearly on the light intensity emanating from the sample, then each part of the object is blurred by the same PSF [10]. In this case, the second part of the integrand (i.e., the PSF) depends only on the relative coordinate $(\vec{r} - \vec{r}')$, and the system is called linear shift invariant (LSI). Equation 1.10 is then simply a convolution. The imaging process can

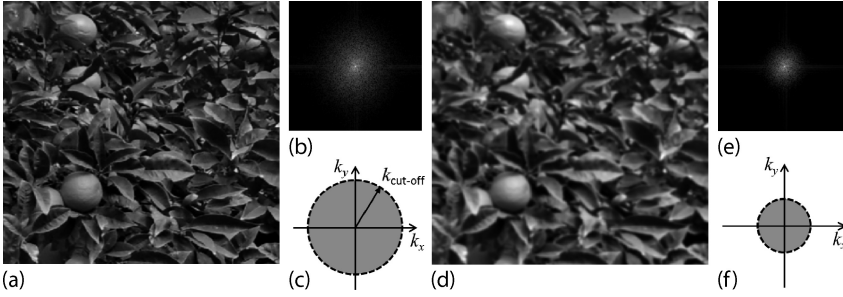


Figure 1.2 Details from two photographs of a mandarin orange tree. The left part depicts the high-resolution data (a) and its Fourier transform (b). In the representation of the Fourier transform, a decomposition of image (a) in terms of “spatial frequencies” is done. Average intensity and slowly varying image features are represented in the center, while fine details (small structures) are

located toward the periphery. A schematic of the frequencies present in the image is illustrated in (c). The right part shows the same data recorded with lower resolution, i.e., with increased blur (d), together with its Fourier transform (e). The reduction of fine structural details (i.e., lack of high-frequency content) is apparent from the schematic outline of the spatial frequencies present (f).

now be described using the Fourier transforms G and F of g and f , respectively:

$$G(\vec{k}) = F(\vec{k}) \text{OTF}(\vec{k}). \quad (1.11)$$

In this equation, OTF is the Fourier transform of the intensity PSF, the so-called *optical transfer function* (OTF), and k is the spatial wave vector (or spatial frequency). Because of diffraction, fine structural details are not transmitted in a microscope. Thus, the PSF is band-limited, which means that the OTF is zero for high frequencies beyond a cut-off frequency $k_{\text{cut-off}}$. This is schematically illustrated in Figure 1.2: Two versions of a photograph are shown (a) and (d) together with the respective strength of the Fourier transforms (b) and (e). The concept of the spatial frequencies present in the image are depicted in (c) and (f) respectively. The crisper image data (a) can be associated with a broad range of spatial frequencies present, indicative of a “broad” OTF of the imaging system. In contrast, an image taken at low resolution (b) has a much narrower OTF. The regions in which the OTF is non-zero (or above the noise level) is referred to as the “support” of the OTF. The cut-off frequency can also be used as a measure for the resolution of the microscope system. In analogy to the considerations by Ernst Abbe, the cut-off frequency of an optical microscope is given by $k_{\text{cut-off}} = \pi \text{NA} / \lambda$.

1.1.1

Examples of Microscopic Imaging without Using Visible Light

Ernst Abbe developed his famous formula by considering scattering arising from a sample itself in a manner similar to a Fourier decomposition of the sample structure [11]. For the sample structure to be imaged, the minimum requirement is that the ± 1 order of the scattered signal must be detected by the objective lens.

The same formula can be derived from general considerations on diffraction in the context of matter waves, in which case the wavelength used for imaging, i.e., the wavelength for the detection of the contrast, is given by the de Broglie wavelength [12]. Equation 1.2 can be used, for example, to calculate the resolution in electron microscopy (EM) [13]. For an acceleration voltage of 75 keV, a de Broglie wavelength of approximately 0.22 nm was originally calculated [14], indicating that the resolution is orders of magnitude better than for optical imaging, and much more detail may be observed in electromicrographs. An additional relativistic correction must be made to account for the electron velocity approaching the speed of light, c :

$$\lambda_{e^-} \approx \frac{h}{\sqrt{2m_0E \left(1 + \frac{E}{2m_0c^2}\right)}}, \quad (1.12)$$

with h being Planck's quantum, m_0 the rest mass of the electron, and E the acceleration voltage applied.

In addition to these diffraction-based imaging approaches in transmission electron microscopy (TEM) [14], other microscopy techniques that do not rely on visible light either have been established. These include, for example, scanning tunneling microscopy (STM) [15] and atomic force microscopy (AFM) [16]. All of these non-optical techniques place a number of restrictions on samples. Some of the more severe disadvantages, for instance, in using electron microscopy (EM) are that experiments are generally performed with the samples placed in a vacuum, which requires a special sample preparation, and often coating with a metal film is also necessary. Nonetheless, these techniques played a major role in the discovery of essential elements of chromatin nanostructure, such as the nucleosomes [17, 18] and other important features (for review see [19]).

All microscopy techniques that avoid the use of visible light have in common that it is not easy to label and distinguish multiple types of targets inside cells, so it is difficult to achieve specific contrast. Typically, immunostaining using gold nanoparticles can be done for EM; however, before the advent of electron spectroscopic imaging (ESI), there was no easy way to perform energy-discriminating imaging (i.e., to use different wavelengths in the same acquisition sequence), and so the number of different spectral signatures was severely limited. Modern TEM allows energy filters to be used, which produces a contrast for specific chemical elements. In biological tissue, a number of different chemical elements can be used for discriminating imaging. However, each of these elements of which biological tissue is composed is typically found simultaneously in a plethora of proteins, lipids, amino acids, and others alike and is thus not specific. Early approaches of electron spectroscopic imaging of the nucleus made use of phosphorus and nitrogen mapping, providing sufficient contrast and resolution to distinguish protein-based from nucleic acid-based supramolecular structures [20]. Last but not least, the irradiation of a sample with accelerated electrons gives rise to ionization, which in turn correlates with structural changes within the sample such as atomic displacements, migration, and desorption effects [21].

For the aforementioned reasons, and in comparison to EM, fluorescence microscopy has a couple of advantages: (1) multiple specific cellular components may be observed from within the same sample through molecule-specific labeling and (2) the requirements for sample preparation and observation are modest. Although it is not necessarily true for all advanced super-resolution light microscopy realizations, in principle light microscopy allows the observation of structures inside a live sample in real time. As a consequence, light microscopic techniques play a vital role in the life sciences.

1.1.2

Early Concepts of Enhanced Optical Resolution

Once the theoretical resolution of microscopic detection was understood, work related to the further optimization of microscopic illumination started. Shortly after Abbe, realizing that the final microscopic image resolution also depended on the coherence of the illumination light, August Köhler achieved precise control over the illumination. Despite this, it took some time to realize that the effect of illumination can, in principle, be used to even enhance the resolution beyond the theoretical limit given by diffraction in microscopic detection. On November 7, 1957, Marvin Minsky filed a US patent application on the construction of a *confocal microscope* [22]. The basic idea was to focus a strong light source point by point onto a sample, thereby scanning an object with a focused beam and to register the transmitted/reflected light also point by point. For enhanced resolution, a pinhole in front of the light detector rejects light originating from sample parts above and below the focal plane. At the time, however, the laser was yet to be invented, and Minsky's concept for a transmitted/reflected light confocal microscope, called a "microscope apparatus," remained largely unnoticed until the 1980s. Only upon equipping the instrument with suitable laser light sources did the then termed "confocal laser scanning microscope (CLSM)" become a valid alternative to conventional microscopy [23, 24], with its tremendous success especially in the fluorescence mode.

The basic principle of CLSM is illustrated in Figure 1.3. The "point source" obtained from a laser light source may be focused with high efficiency as a diffraction-limited spot into the focal plane of the objective lens. This small spot may be scanned within the focal plane, for example by a set of mirrors, and at each scan position the fluorophores subjected to illumination by this focal spot emit fluorescence, which is collected by the objective and directed to the detector. Typically a single-element detector, such as a photomultiplier tube (PMT) or a highly sensitive photodiode, is used, requiring descanning of the detected light in order to be able to direct the fluorescence signal collected by the objective lens towards the point detector. This is achieved by having the scanning device (e.g., the scan mirrors) not only in the illumination but also in the detection path. By moving the scanning mirror (or alternatively by moving the sample), the position of the focused diffraction-limited illumination spot is changed and the fluorescence signal from neighboring "pixels" is recorded.

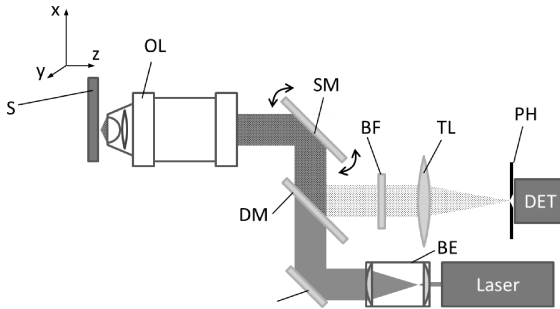


Figure 1.3 Schematic representation of a confocal laser scanning microscopy (CLSM) setup. Laser light sources for fluorescence excitation are collimated and expanded using a beam expander (BE) of fixed or variable output beam width. The beam is subjected to a scanning mirror (SM) device, typically with two rotating mirrors for deflecting the beam in the x - and y -directions. The excitation beam illuminates the back focal plane of an objective lens (OL), resulting in a diffraction-limited illumination spot within the focal plane of

the OL, i.e., within the sample. Fluorescence light is collected via the same OL and descanned on the SMs before it is separated from the excitation light by a dichroic mirror (DM). Residual laser light is suppressed by a blocking filter (BF). A tube lens (TL) focuses the fluorescence light onto a pinhole (PH) to prevent out-of-focus light from entering the detector array (DET). An equivalent setup without an excitation PH was proposed by Cremer and Cremer in 1978 [23].

The light intensity of the illumination (excitation) focal spot is distributed according to the illumination PSF. If – in an ideal situation – the back focal plane of the objective lens is fully illuminated with equal intensity, corresponding to a circular aperture, the PSF displays a pattern according to Equation 1.3 with a central “Airy disk” (Figure 1.1) having a radius proportional to λ/NA . The overall probability of detecting a fluorescent molecule that is in the focal plane but positioned off-axis, i.e., not centered in the PSF, is given by the product of the probability of exciting it times the probability of detecting it. While the former is given by the illumination PSF_{ill} , the latter is given by the detection PSF_{det} , and the total PSF_{tot} is given by

$$\text{PSF}_{\text{tot}} = \text{PSF}_{\text{ill}} \times \text{PSF}_{\text{det}} . \quad (1.13)$$

As with conventional wide-field microscopy, the resolution of a CLSM is determined by the width of the PSF. Additionally, the scanning (displacement of the focal spot) needs to match the width of the PSF: The smaller the focal spot is, the more meaningful pixels can be acquired in the image, and each pixel will contain information from a smaller region in the sample. As a consequence, the image will be less blurred. While the confocal microscope is mostly used for its ability to suppress out-of-focus light [25], theoretical considerations show that the optical resolution can be enhanced by a factor of 1.4 in the object plane [25–27], and a true optical resolution of about one wavelength along the optical axis (i.e., perpendicular to the object plane) can be obtained [28]. For a detailed historical review please see, for example, [29].

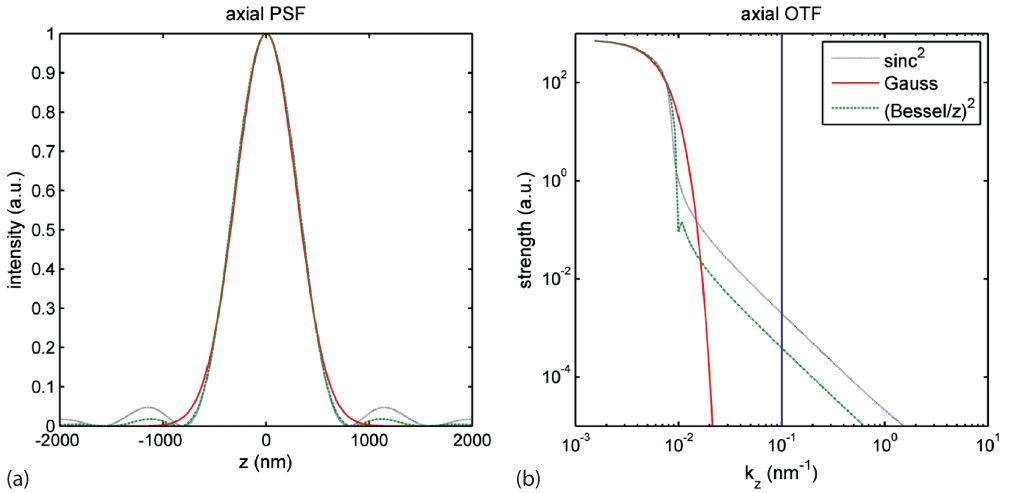


Figure 1.4 Effects of type of illumination beam on OTF. Ringing or oscillating intensity distributions (a) have a significant effect on the transfer of higher spatial frequency components (b), although the FWHM for all three intensity distributions is the same. Gaussian intensity distributions result in a loss of more than one order of magnitude at

high frequencies. However, the spatial frequencies corresponding to ca. the FWHM of the axial PSF ($k_z \approx 1.25 \times 10^{-2} \text{ nm}^{-1}$) are much more efficiently transmitted for Gaussian beam profiles. The cut-off frequency for axial imaging using a wide-field system (given by $k_z = \pi \text{NA}^2 / [(n - \text{NA})\lambda]$) is indicated by the vertical blue line.

Thus it was discovered that differently shaped illumination beams clearly have an effect on resolution (which might be obtained in terms of the FWHM of the resulting total PSF). From an analytic point of view, it is also important to know exactly how the OTF is affected using different beam shapes. Figure 1.4 shows how the strength of the axial OTF depends on the type of illumination used if the direction of illumination forms an angle of 90° with respect to the detection axis, i.e., the illumination beam enters parallel to the object plane. This configuration is realized, for example, in light-sheet fluorescence microscopy (described in Chapter 7). The cut-off frequency beyond which structural information cannot be transmitted due to diffraction may be given by $\pi \text{NA}^2 / [(n - \text{NA})\lambda]$ [30]. It can be seen that oscillating illumination patterns such as the function $((\text{Bessel}J_1(z)/z)^2)$ and the axial PSF $(\text{sinc}(z)^2)$ result in superior transmission of very high spatial frequencies compared to the Gaussian beam profile, whereas for lower spatial frequencies, the Gaussian beam profile seems to be advantageous. It is therefore evident that resolution alone might be an insufficient criterion for judging the quality of an imaging system since the amount of noise present in acquired individual images has different effects on the final resolution for differently shaped illumination beams. An alternative approach is to use the *contrast-to-noise ratio* (CNR) as an additional criterion for image quality, which also takes into consideration how the contrast is affected by the noise level [31].

1.1.3

Two-Photon and Near-Field Optical Microscopy

A common problem of conventional and confocal fluorescence microscopy is the photobleaching of dyes [32–34]. Not only does it limit the recording time, but bleached dye molecules may result in phototoxicity and additional chemical reactions and, thus, inflict damage on samples and affect microscopic observations, in particular of live samples. By the use of two-photon excitation, fading in the sample can be limited to a small volume owing to the spatial confinement of the two-photon process, and as a consequence, the bleaching of the fluorophores can be reduced in a suitable excitation-detection scheme. Often, two-photon excitation is implemented in a point-scanning configuration, and light is detected only from a small focal volume surrounding the geometrical focus of the detection (single-element detector) [35]. Other approaches to realizing the confinement of excitation to the focal plane make use of multi-point or line scanning or temporal focusing [36–38]. Typically, a short laser pulse duration ensures that the average radiation energy remains low, so that damage to the specimens is avoided.

In addition to a decrease in the overall photobleaching of samples and the reduction of phototoxic damage, the non-linear multi-photon process of optical absorption, which limits the excitation to the focal point, provides further benefits in comparison to single-photon microscopy: The use of infrared (IR) excitation results in a deeper penetration depth into a sample because the IR light interacts less with the tissue. The pinhole usually employed in CLSM can generally be dispensed with since in multi-photon excitation fluorescent light is generated only within a small, well-confined volume.

Another way to achieve subwavelength resolution and imaging is based on coupling the light to/from specimens via an optical element that is located a subwavelength distance from the sample, i.e., on probing the *near field* of the light emitted by the sample, or by placing the sample in the near-field of the illumination. Typically, such a probing optical element is realized by a light guide, for example, a glass fiber, although other experimental layouts have been used (e.g., [39, 40]). When the probe is less than one wavelength from a specimen, the resolution is given by the size of the aperture and not by the wavelength used for imaging [41]. In 1984, Pohl *et al.* demonstrated near-field imaging in the visible wavelength region and showed that subwavelength resolution imaging (down to ~ 25 nm) was possible by employing a probe with an extremely narrow aperture that was scanned along a test pattern [42]. Around the same time, similar approaches were followed by another group [43, 44], which published work on the development of a microscope setup capable of 500 Å spatial resolution.

1.2

Methods to Circumvent the Classical Resolution Barrier in Fluorescence Microscopy

Previously, a number of light microscopy approaches have been developed with the aim of getting around the classical resolution limit. Such imaging methods with an effective resolution below the Abbe limit are referred to as “super-resolution” microscopy; this term was coined by Toraldo di Francia [45]. In what follows, the text will focus on super-resolution in the context of far-field fluorescence microscopy. In principle, there are four concepts on which present super-resolution approaches rely:

- Methods to extract meaningful structural information are based on assumptions on fluorophore distribution. Generally, fluorophores (or targets labeled with them) cannot take any arbitrary position within a sample. Such methods can be implemented based on models of the emitter distribution [46, 47] or based on statistical inference (e.g., Bayesian induction) [48]. Since these methods do not enhance the optical resolution but provide a likely super-resolution representation for an unknown structure, they will be discussed only in special cases. It should be noted, however, that a reconstruction obtained in this way is only *one* of the very many possible configurations, but indeed a very likely one. For similar reasons, deconvolution approaches will not be discussed either.
- Particle tracking. Probing a structure with a limited number of sources (typically one) in a dynamic setup allows the observer to follow the trajectories of single particles (e.g., due to thermal motion) with super-resolution. Thus, accessible spaces may be reconstructed, resolving the surrounding matrix structure.
- Methods to increase dimensionality of acquisitions [49]. These provide a basis for additional discrimination of fluorescence signals, even if their (diffraction-limited) signals overlap to a large degree on the detector. Practical approaches to increasing the dimensionality in fluorescence microscopy have recently been termed *localization microscopy* because in quantitative imaging, the precise location of the emitter is extracted. In reference to the discrimination of fluorophores based on their emitting/non-emitting state, some of these methods are also known under the heading *stochastic switching*. The localization microscopy approaches will be discussed in Chapter 5.
- Methods to decrease the volume from which fluorescence is emitted. Some of these methods allow for a true resolution enhancement by effectively shrinking the volume of the total microscope PSF. They generally require a special type of illumination. Paradigmatic for this type of approach are, for example, 4Pi- and STED confocal laser scanning microscopy (Chapter 6), which are members of the family of super-resolution methods based on *targeted switching*. But approaches of structured illumination microscopy (SIM) or patterned excitation microscopy (PEM) also reduce the volume from which fluorescence is detected; they are discussed in Chapter 4.

The last two methods are often jointly implemented in one of the SRM approaches. For instance, the interferometric detection of a fluorescence signal by

means of simultaneous detection through two objective lenses (4Pi configuration) can be employed to extract additional position information based on the phase of the detected fluorescence light. Similarly, color discrimination, fluorescence lifetime discrimination, or polarization discrimination in emitted fluorescence light can be used to increase dimensionality. Discussion of many of these approaches will be geared toward but not limited to the context of localization microscopy (Chapter 5). The underlying concepts are introduced in what follows.

1.2.1

Interferometric Microscopy

The optical resolution achieved with a confocal and two-photon microscope (“2P microscope”) is too low for many practical applications. By analyzing the formulas for the resolution of the microscope, a potential route to arriving at an enhanced optical resolution can be derived, namely, by increasing the numerical aperture (NA) of the microscope [50]. The need for increasing the numerical aperture led to the development of microscopes employing a coherent use of two objective lenses, in particular the 4Pi CLSM [51], the wave-field microscope [52–54], and the I⁵M microscope with a significantly higher resolution along the optical axis [55]. These three microscope techniques make use of two opposing lenses and a coherent overlay of the illumination or detection signal, respectively, to boost the effective opening angle used for imaging. The concept of coherent detection using a set of two objective lenses is schematically illustrated in Figure 1.5.

Other forms of interferometric illumination along the image plane have been employed to circumvent the need for (coherent use of) a second objective lens; these methods are generally termed SIM [57, 58]. All of these first super-resolution techniques necessarily relied on digital image processing and yielded resolutions down to approximately 100 nm in the direction in which the interference pattern was modulated. The concept of the coherent use of two objective lenses, however, has been transferred to and combined with other advanced optical microscopy techniques.

Wave-Field Microscopy

A particular configuration of interferometric illumination is obtained when the illumination pattern is aligned in the axial direction: The principle of spatially modulated illumination microscopy and wave-field microscopy (or standing-wave microscopy), a particular form of axially structured illumination microscopy (Section 4.1), is to bring two coherent, usually collimated, linearly polarized laser beams of equal intensity to constructive interference in the object space of a microscope, for instance by placing the sample between the objective lens and a mirror [59]. This creates a standing wave with fixed intensity minima and maxima, resulting in a selective excitation in the object space at the positions of the intensity maxima. Thus planes with maximum intensity occur at equidistant positions perpendicular to the plane of incidence of both beams and parallel to the half-angle between the two laser beams. The concept of a microscope system with such an

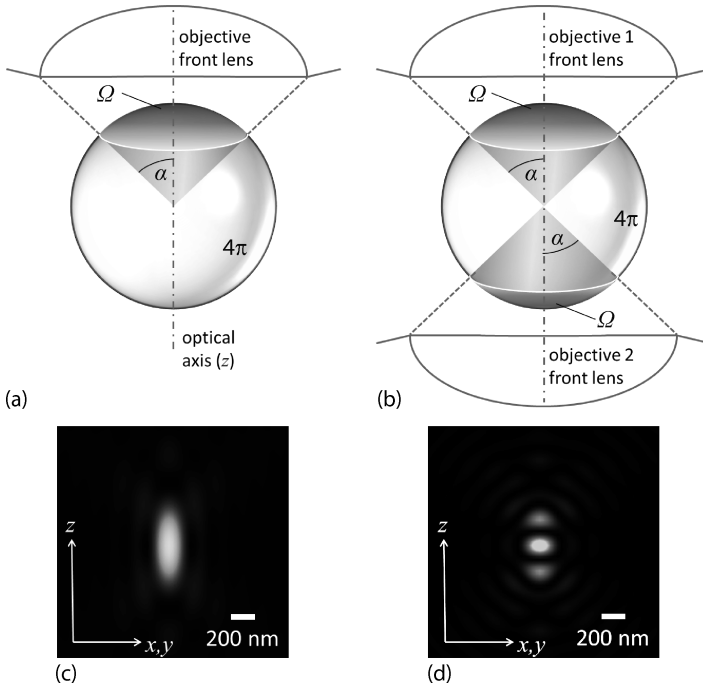


Figure 1.5 Detection of fluorescence signal using an objective lens leads to the well-known blur of the image [7]. (a) Fluorescence light is emitted from the sample in all directions, for example, in the form of a spherical wavelet. However, only a fraction of this light (corresponding to a “cap” of the spherical wavefront within the acceptance cone of the objective lens) is detected. The acceptance cone is usually defined by the half-angle α , but it can also be characterized using the solid angle Ω . The solid angle of a full sphere equals

4π . (b) More light can be detected using two objective lenses. (c) The diffraction pattern of a single objective lens is typically elongated along the optical axis (z), i.e., along the direction of viewing. (d) If the focal positions of the two objective lenses coincide and the path lengths of the light beams on either side are adjusted, a symmetric interference pattern along the optical axis can be observed, with the central maximum being much narrower compared with the diffraction pattern observed when using a single objective lens [56].

illumination scheme was investigated several years before the laterally structured illumination microscope was developed. For the case in which the maximum intensity planes are oriented perpendicular to the optical axis, this technique was described in [52, 60].

For the experimental realization of this technique [53] it was assumed that along the coordinate given by the optical axis (i.e., in the direction of observation), only one fluorescently labeled target is present (see earlier: assumptions on the fluorophore distribution). Furthermore, the object to be examined had to be thin so that there would be no ambiguity as to which wave front maximum of the standing wave-field should be assigned to the position of the object. It was found that these requirements rendered the approach in its original form impractical for general use. However, the conceptual design of the use of wave-field illumina-

tion in fluorescence microscopy was an important step since it paved the way for the development of advanced optical imaging techniques such as I⁵M and SIM.

1.3

Implementation of Super-Resolution Microscopy

The principles of SIM outlined earlier can be used to extract structural information beyond the resolution limit without providing actually enhanced optical resolution. These concepts will be discussed in Section 4.1 on axially structured illumination. The key point in recent microscopy developments aimed at achieving spatial resolutions *far* beyond the diffraction barrier is to either exploit in a presently stochastic way the properties of fluorescent probes (e.g., binding, photoswitching, activation) or arrive at a fluorescence emission that responds in a non-linear way to the illumination intensity. To realize such phenomena, a number of approaches have been proposed relying, for example, on the use of (photo-) activation [61] or cis-trans isomerization [62] of fluorophores, or on the saturation mostly of electronic transitions, as in saturated excitation (SAX [63–65], saturated disexcitation (STED) ([66]), and saturated ground state depletion (GSD) ([67]). Common to all of these techniques is the existence of a state of the fluorophore (or pairs of fluorophores) in which it (or they) cannot be excited (e.g., the already excited state in SAX, the ground state in pulsed excitation STED, the T₁ triplet state in GSD), or in which it does (or they do) not emit fluorescence in the detection channel (e.g., the non-activated state in PALM [61], red-shifted stimulated emission in STED [66], shifted emission spectra in fPALM [68], quenched fluorescence in stochastic optical reconstruction microscopy (STORM) [62], unbound dye in binding-activated localization microscopy (BALM) [69]), or blinking/bleaching of the dye in generalized single-molecule high-resolution imaging with photobleaching (gSHRIMP), nanometer-localized multiple single-molecule fluorescence microscopy (NALMS), direct STORM (dSTORM), spectral position determination microscopy (SPDM), Bayesian analysis of bleaching and blinking (3B), and others) [48, 70–76]. However, the existence of such a state in which fluorophores are not detected is not the only requirement for SRM. The transitions that lead to a population and depopulation of this state also play an important role.

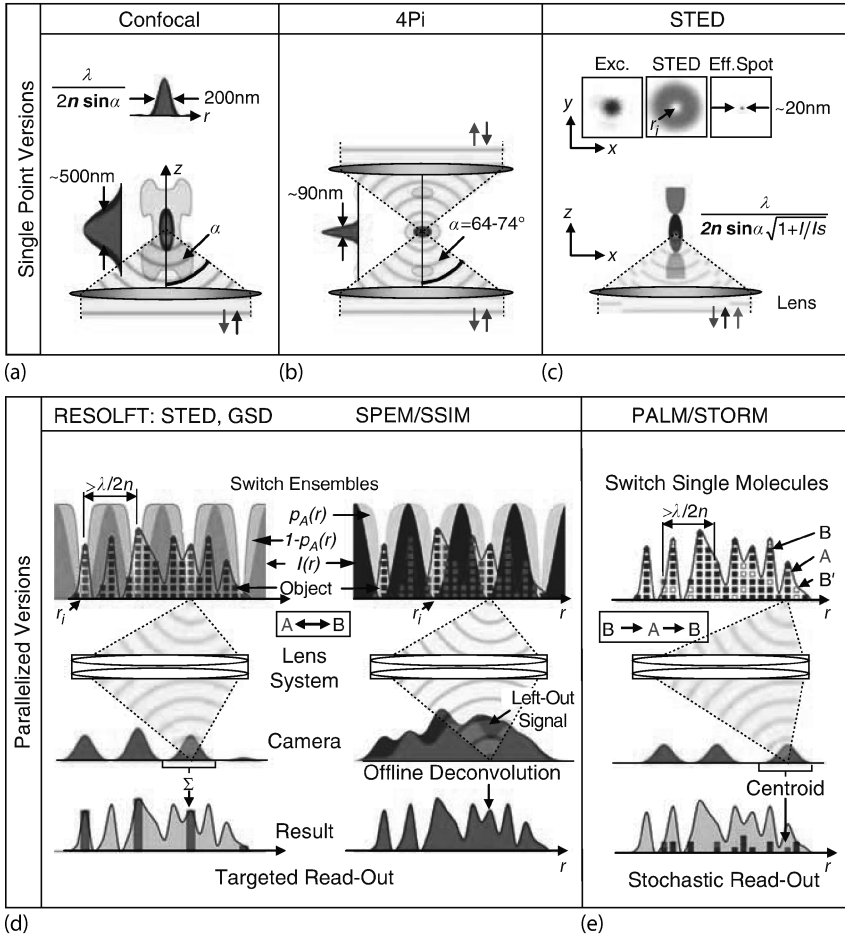
While resolution can already be enhanced using a CLSM system (Figure 1.6a) or a 4Pi CLSM (Figure 1.6b), such microscope devices merely shift the diffraction limit: Up-to-date field-corrected objective lenses (with an opening half-angle $\alpha = 74^\circ$) have enabled dual-color 4Pi recordings with regular one-photon excitation [77, 78]; however, by the application of two-photon excitation using such lenses, a single central spot with a FWHM of $\Delta z \sim \lambda/(3n)$ was observed with negligible sidelobes [79] (Figure 1.6b). Similar values for the axial resolution have been obtained using I⁵M. It uses a detection system like a 4Pi microscope, thereby coherently adding spherical wavefronts caps of the emitted fluorescence light on

the detector. 1^5M – unlike 4Pi – does not focus the illumination, and so offers fast wide-field imaging capabilities. The clearly enhanced values for the z -resolution (FWHM shifted from 400–800 to 70–150 nm) was the first substantial improvement seen in far-field optical microscopy in around 100 years.

Figure 1.6c,d shows the concept of discrimination based on stimulated emission depletion (Figure 1.6c), saturated depletion (Figure 1.6d, left) or saturated excitation (Figure 1.6d, right). The introduction of non-linearities (owing to saturation) allows spatial encoding in the fluorescence signal in such a way that the extent of the region encoded is no longer limited by diffraction. For example, in saturated patterned excitation microscopy (SPEM/SSIM/SAX), the sample is illuminated with a pattern featuring peaks with high intensity alternating with dips with zero intensity. Both the illumination pattern and the detection are limited by diffraction. However, when illuminating using an excitation pattern with very high intensity I_{ill} much larger than a threshold I_s , only those fluorophores within a small region around the area (or areas) of zero intensity are left in the ground state. The position (center) of the area of zero intensity is denoted by r_i . The extent of the area in which fluorophores are not excited can be made much smaller than the typical width of a diffraction-limited spot, i.e., much smaller than the classical optical resolution.

The discrimination of fluorophores based on the separation of their properties in order to arrive at super-resolution is often realized in the form of a stochastic transition (e.g., PALM/fPALM/STORM). Such a separation is straightforward only if the time period between the transitions is much longer than the fluorescence lifetime, allowing the detection of a large number of photons from a single emitter during one of these periods. These concepts are usually summarized under the heading “localization microscopy” and will be discussed in Chapter 5. The key point in these techniques is to measure the center of a few isolated diffraction-limited signals rather than to image all fluorophores together. In the case of imaging isolated fluorophores, the resolution of the final image depends among other things on the accuracy with which the position of the emitting fluorophore can be determined. Figure 1.7 illustrates the relation between the spread in the determined positions (triangles), i.e., the precision of the position determination, and the accuracy of the position measurement. The measured position (barycenter of the scatter) may not represent the true position adequately if other errors, such as mechanical drifts or systematic errors in the extracted positions, are present. However, if we are interested in the configuration or arrangement of a set of sources rather than in their true locations, the accuracy, i.e., the difference between determined position and true position, does not affect the result if the offset is similar for all sources. Only in the case of a variation in accuracy from one source to the next does it need to be considered for the determination of the final error in the measurement.

In some instances, stochastic separation is not required. Neighboring signals labeled with different spectral signatures can be discriminated even if their emitted signals highly overlap on the detector. Potential realizations of such concepts, i.e., super-resolution using photostable fluorophores, will be discussed in Chapter 8.



Structured Illumination Microscopy

In addition to the techniques based on the existence of a non-detectable or non-excitable state, patterned excitation can be employed to effectively shrink the volume from which fluorescence is detected [57, 58]. A “simple” version of this concept, namely focused excitation, is also realized in CLSM, and hence in STED and 4Pi CLSM as well. In principle, any of the contrasting mechanisms reported for fluorophores could be used for SRM if it provides a stochastic or non-linear response, or if it is susceptible to patterned excitation. Such contrasting mechanisms, some of which may not require the use of fluorescence at all, are described in what follows. Other versions of the concept of patterned excitation based on a wide-field detection scheme will be discussed in Chapter 4. An important feature of many practical implementations of SIM (in contrast to most other forms of SRM) is that they can operate in *linear excitation* mode, i.e., the fluorescence emission depends on the excitation intensity in a linear manner. This facilitates quantitative intensity-based measurements enormously [81–83].

◀ **Figure 1.6** Optical layouts and concepts for a number of SRM approaches. (a) Confocal microscopy is shown here as a diffraction-limited reference. The excitation light wave is transformed (by the lens) into a spherical wavefront cap that results in a 3D diffraction spot exciting the fluorophores in the focal region. A point-like detector (not shown) collects the fluorescence primarily from the main diffraction maximum (dark area in center of focus), thereby providing a slightly improved resolution over conventional fluorescence microscopy. Yet the resolution of a confocal microscope is limited by diffraction to an FWHM > 200 nm in the focal plane (x, y) and to >450 nm along the optical (z) axis. (b) 4Pi microscopy improves the z -resolution by coherently combining the wavefront caps of two opposing lenses; the concept renders a main spot featuring an FWHM of 70–150 nm along the z -axis. (c) A typical single-point implementation of a STED microscope uses a focused excitation beam (Exc.) that is superimposed by a doughnut-shaped STED beam to keep molecules dark by quenching excited molecules through stimulated emission. In regions around r_i where the STED beam intensity is beyond a threshold I_s , the STED beam essentially switches the fluorophores off by nailing them down to the ground state. By ensuring that the doughnut intensity I exceeds I_s in a large area, the effective spot in which the fluorophore can still be bright and active is confined to subdiffraction dimensions. Accordingly, a measured 20 nm diameter spot is shown, which is approximately ten times below the diffraction barrier. Scanning such a subdiffraction sized spot across the sample yields subdiffraction images. (d) The concepts of STED, GSD, (left-hand side), and SPEM/SSIM (right-hand side) can be viewed as special cases of a more general concept called “RESOLFT.” A hallmark of this generalized concept is that it utilizes focal light distributions $I(r)$ with zero-intensity points at positions r_i to confine either a bright (A) or a dark fluorophore state (B) in space. The zeros are preferably $>\lambda/(2n)$ apart in the focal plane. Two examples of this generalized concept are shown. Left: the intensity drives a transition $A \rightarrow B$ to confine the bright state A in space. This is the case for a parallelized STED, GSD, or RESOLFT approach using reversibly photoactivatable

proteins or photochromic dyes. Right: in the SPEM/SSIM concept, the intensity $I(r)$ drives a transition $B \rightarrow A$ that confines the dark state B in space. In both cases, the positions of state A or B are predefined in space by $I(r)$ and r_i . When imaged onto a camera the steep regions of state A (left) or state B (right) become blurred. However, the diffraction blur can be dealt with (as shown in the left-hand panel STED, GSD) by allocating the signal (from the diffraction blob) to the known coordinate r_i of the zero in the sample space. The image is gained by scanning the array of zeros (r_i) across the sample and recording the fluorescence for each step. The diffraction blur can also be dealt with for SPEM/SSIM (right-hand panel) because the super-resolved data are encoded in the steeply confined dark regions around r_i of state B. Since SPEM/SSIM initially produces a so-called negative data set, the SPEM/SSIM image is finally obtained by mathematically converting the negative data set into a positive one. The small boxes in the sketches symbolize the fluorophore molecules that make up the object. $p_A(r) \leq 1$ defines the normalized probability of occurrence of state A. Although all these RESOLFT concepts are suitable for detecting single molecules, they generally operate with ensembles. Since the position at which the fluorophores are in A or B – and hence emitting – is predefined by the zero-intensity points r_i , the RESOLFT strategy has also been called the *targeted read-out* mode. (e) The single-molecule switching concepts (e.g., PALM/STORM) do not define the region from where a signal is emitted but read out the fluorophores of the object stochastically, molecule by molecule. Individual fluorophores are sparsely switched to a specific bright state A that is able to emit $m \gg 1$ photons before the molecule returns to B. The detection of $m \gg 1$ photons enables the calculation of the centroid of the diffraction blob of individual molecules when imaged onto a camera. Thus it is possible to assemble an image consisting of centroid position marks with a statistically variable resolution depending on m . The concepts (c–e), i.e., STED, GSD, RESOLFT, SPEM/SSIM, and PALM/STORM, are not limited by diffraction, meaning that they can resolve similar molecules at nanometer distances. Reprinted from [80], © 2010, with permission of Springer.

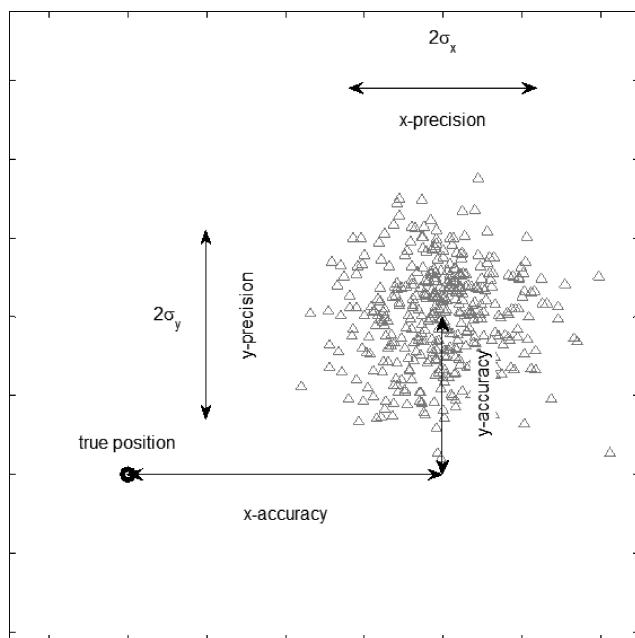


Figure 1.7 Precision and accuracy in repeated measurement of position. Hemmer and Zapata posit [84] that precision is a measure for repeatability while accuracy is the distance between the measurement result (the barycenter of the scattered locations) and the true position. For large sample sizes, it is

a measure of the systematic error, whereas for small sample sizes (i.e., only a single or a few position measurements for each emitter), it also encompasses precision. Triangles: data points (i.e., measured locations); circle (bottom left): true position.

Non-Linear SIM

The resolution enhancement in patterned excitation can be further increased by inducing a non-linear response of the fluorophore emission to the illumination intensity. An example is to saturate the excited state by the application of high-intensity illumination. Such methods are termed “saturated excitation microscopy” (SAX), “saturated patterned excitation microscopy” (SPEM), or “saturated structured illumination microscopy” (SSIM) [63–65] (Figure 1.6d).

An additional possibility for implementing non-linear SIM requires the use of photoswitchable fluorophores (Section 2.3). Photo-switching/photoactivation is an inherently non-linear process and can be employed as an alternative to saturation for super-resolution imaging. Owing to the low light intensities needed to switch the molecules [85–88], super-resolution images can be obtained over prolonged periods of time with much less risk of inducing photodamage. Photoswitchable fluorophores can be reversibly switched between two distinct absorption/emission states using light. A non-linear response of the fluorescence emission to the illumination intensity can be obtained by saturation of either of the two population states. In the case of non-linear SIM, a second standing-wave interfer-

ence pattern is applied for non-linear targeted switching of the dye molecules, so that the fluorescence signal is obtained from a drastically reduced volume only [89].

Super-Resolution Optical Fluctuation Imaging

Another technique that in principle does not rely on the existence of a non-detectable or non-excitabile state of the fluorophore is super-resolution optical fluctuation imaging (SOFI) [90] (Section 5.7.3). SOFI requires the use of dyes with repeated cycling between at least two different emission states. Until now, these states have been the fluorescent and non-fluorescent state (emission “on” and emission “off”). Owing to the fact that SOFI is based on the independent fluctuations of emitters, no activation or induced photoswitching step is required.

Reversible Saturable Optically Linear Fluorescence Transitions (RESOLFT)

Instead of saturated excitation as in SAX/SSIM/SPEM, it is also possible to employ saturated disexcitation of fluorophores to obtain a non-linear response to the applied illumination intensity. Using low illumination intensities, the necessary photoswitchable fluorescent probes can undergo a reversible transition between a fluorescent “on”-state and a fluorescent “off”-state. As such, RESOLFT is a generalized version of STED microscopy, in which an additional laser beam is used to deplete the fluorophores at the periphery of the excitation into the dark “off”-state.

For RESOLFT and non-linear SIM based on photoswitchable fluorophores, but also for SOFI and even for a Bayesian analysis of blinking and bleaching [48], the requirements on the fluorophores and the factors determining the resulting resolution are similar. The reversible switching between the two states of the fluorophores must be efficient and repeatable for many cycles in order to reliably discriminate neighboring fluorophores. The resolution of the resulting images is inversely proportional to the square root of the number of switching cycles, i.e., in order to enhance the resolution by a factor of 10 requires the fluorophores to switch states 100 times. Only a small selection of the presently available reversible switching proteins are able to live through this many cycles; switching fatigue is therefore a limiting factor in imaging techniques relying on photoswitchable fluorophores.

Stimulated Emission Depletion (STED) Microscopy

An implementation of focused SRM is STED microscopy. In contrast to the microscopies relying purely on structured illumination for excitation, it also employs structured illumination for disexcitation. Thus, it not only shifts the resolution limit of microscopic imaging but completely overcomes it [66, 91] and limits the resolution of the final images only by the signal-to-noise ratio and optical aberrations. Usually based on a point-by-point CLSM approach, additional fluorescence depletion (stimulated emission depletion) of the peripheral areas of the illumination spot results in a resolution of less than 100 nm in all three spatial directions of space even in dual-color experiments [92]. The technique of STED is very special

in that it employs all of the concepts required for SRM: It uses patterned excitation (usually by a diffraction-limited spot in point-scanning STED) and patterned de-excitation (a diffraction-limited so-called doughnut beam), a shift in the emission spectra (the process of stimulated emission typically results in the generation of far-red photons), and possibly a non-excitable state (the ground state, which is no longer excitable because the excitation pulse is over), at least in first-generation STED and gated STED.

As indicated earlier, the transitions between the states of fluorophores play a crucial role not only in STED but also in other forms of SRM. One of the main purposes of this contribution is to discuss the joint prerequisites for super-resolution in terms of hardware, software, and physicochemical requirements. These topics will be covered in Chapters 2 and 3, irrespective of the actual implementation or particular method of SRM. However, hardware used mostly in STED setups will be discussed in Chapter 6 dedicated to STED microscopy. The assembly of hardware components for STED microscopy is possibly the most challenging. A detailed description of the implementation of STED together with the specifics of sample preparation, including the selection of fluorophores, can be found in Chapter 6.

STED microscopy, along with other methods of SRM, relies on an induced optical isolation of the detected signal. Typically, this is accomplished by a discrimination of the fluorescent molecules based on their properties, i.e., founded on their spectral states (e.g., switching of the fluorophores between on/off, fluorescence observed in different emission channels, different fluorescence lifetimes). Switching a fluorophore requires two states: a detected state A (“on,” bright, fluorescent) and a state B that is invisible with respect to the detection channel (“off,” dark, non-fluorescent); in many cases, both states are connected by a transition. Figure 1.8 shows several states in a fluorophore that are suitable for such transitions. In STED microscopy, the transition between the fluorescent singlet state S_1 and the ground state S_0 is used, i.e., a pair of bright (emitting) and dark states (non-emitting).

Spectral Precision Distance Microscopy

Enhanced structural information content of biological samples is a desideratum. In addition to strategies based on the narrowing of the microscope PSF (or of its FWHM) as in STED microscopy [66] or concepts relying on the reconstruction of the fluorescent structure based on the localization of the individual fluorescent molecules [61, 62, 68], the desired topological and size information of fluorescently labeled objects may well be obtained by other far-field optical microscopy approaches. For instance, the method of spectral precision distance microscopy (SPDM) [93–99] allows for the measurement of object configurations in structures that have extensions less than the wavelength used for imaging. The technique relies on labeling different components of the structure with fluorescent markers of different “spectral signatures” [100], so that several of the sub-components can be simultaneously recorded and discriminated if their excitation/emission spectra [93, 97] or their fluorescence lifetimes [101, 102] differ. The

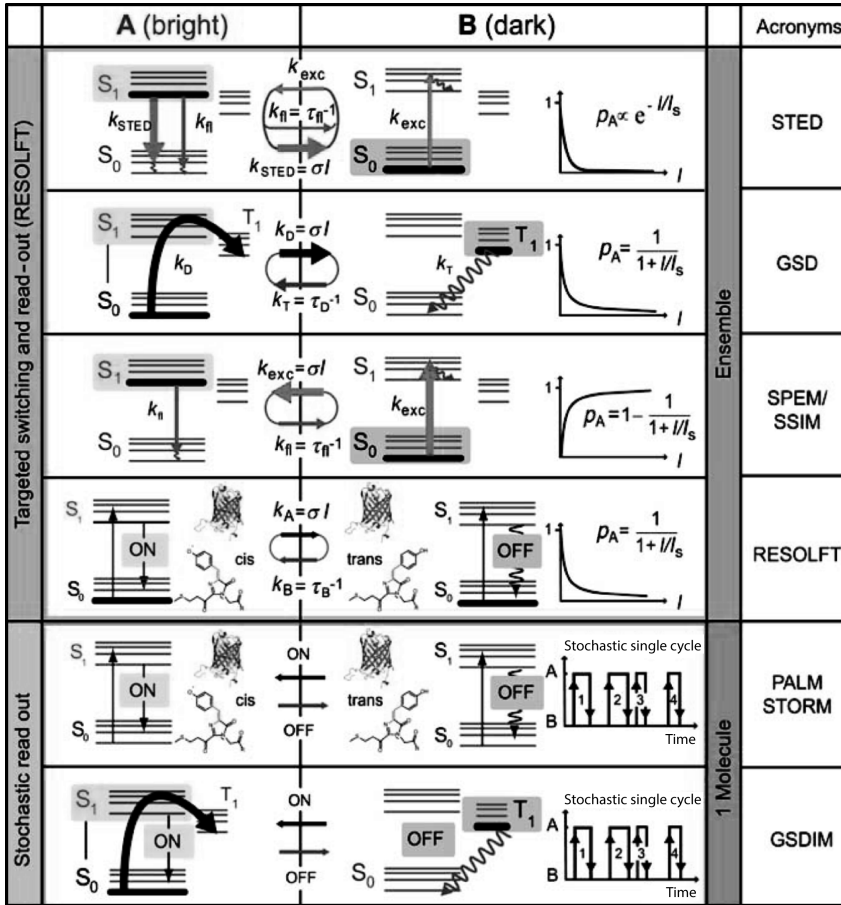


Figure 1.8 Molecular transitions and states utilized to circumvent the diffraction limit. Each nanoscopy modality resorts to a specific pair of bright and dark states. Several concepts share the same states but differ by the direction in which the molecule is driven optically (say $A \rightarrow B$ or $B \rightarrow A$) or by whether the transition is performed in a targeted way or stochastically. The targeted read-out modality drives the transition with an optical intensity I and hence operates with probabilities of the molecule being in A or B. This probability depends on the rates k of transition between the two states and, hence, on the applied intensity I . The probability p_A that the molecule will remain in A typically decreases as indicated in

the panel. $p_A \ll 1$ means that the molecule is bound or “switched” to state B. This switching from A to B or vice versa allows the confinement of A to subdiffraction-sized coordinates of extent Δr at a position r_i where $I(r)$ is zero. In the stochastic read-out mode, the probability that state A will emerge in space is evenly distributed across the sample and kept so low that the molecules in state A are further apart from each other than the diffraction limit. An optically non-linear aspect of the stochastic concept is the fact that the molecules undergo a switch to A from where they suddenly emit $m \gg 1$ detectable photons in a row (a *fluorescent burst*). Reprinted from [80], © 2010, with permission from Springer.

positions of objects are extracted from their coordinates in the 3D image data stack. With conventional resolution fluorescence microscopes, already distances of about 15 nm and higher were measured between such fluorescently labeled objects with a precision (95% confidence interval) of approximately 10 nm [96, 103]. Theoretical calculations consolidate the lower limit for the accuracy of this method to be in the order of a few nanometers, i.e., well below the conventional resolution limit [93, 98].

1.4

Contrast

The tremendous success that fluorescence microscopy has had in biomedical research during the last 50 years is largely based on the stunning contrast that is obtained by attaching fluorescence labels specifically to the structure of interest and consequently detecting only structures that were adequately labeled on a virtually non-existing (i.e., zero) background signal. Fluorophores, which are responsible for the increased contrast in these labels, are sometimes also referred to as *chromophores*. When speaking of chromophores, we stress that the molecule is capable of absorbing light in a specific, narrow band of wavelengths, which is the reason for the observed color. While the term *chromophore* implies that the molecule absorbs light, the terms *fluorophore* and *fluorescence* relate to the process of emitting light [104]. In the primary microscopic contrasting scheme using fluorescence molecules, the dissipation of energy from excited vibrational and rotational states of the fluorophore is used to separate the (red-shifted) emitted light from the excitation light.

In recent decades, several additional contrasting methods have been derived based on the photophysics behind fluorescence in biological samples. A large number of parameters and processes have an influence on the fluorescence emissivity, and in principle any parameter or process having an effect on the fluorescence emission can be applied as the contrasting mechanism. Consequently, a variety of fluorescence microscopy/spectroscopy techniques have been developed that make use of different contrasting mechanisms. Factors that characterize fluorescence emissivity can include the following:

- **Absorption Cross Section:** Fluorophores are generally optimized to yield the highest fluorescence intensity upon illumination. The *absorption cross section* depends on the electron configuration of molecules, but also on their orientation with respect to the *polarization* state of the incident light. The small cross section of two-photon/excitation is the reason why the generation of fluorescence can be restricted to occurring only within the laser focus, providing an alternative means for optical sectioning. However, the success of two-photon microscopy is attributed mostly to its use of IR light, which penetrates deeper into tissue.
- **Quantum Yield:** The probability that fluorescence will be emitted following excitation of a fluorophore is given by its quantum yield. Non-radiative dis-

excitation processes (e.g., a non-elastic collision with surrounding molecules) compete with the fluorescence emission decay. A change in quantum yield is observed in two characteristic fluorescence contrast schemes: quenching and energy transfer.

- **Quenching:** A fluorophore may be put in a chemical or structural configuration such that the electron configuration is unfavorable for the emission of fluorescent light by this particular fluorophore.
- **Energy Transfer:** If the structural configuration is such that one fluorophore forms a joint electronic system with a neighboring fluorophore (of a different type ideally emitting fluorescence with a wavelength further toward the red end of the spectra), there is a chance that Förster resonant energy transfer (FRET) will occur, depending on the spatial separation of the two molecules. The process becomes highly unlikely when the distance between the two molecules exceeds several nanometers. While in this case also the fluorescence emission is quenched, a simultaneous rise of the fluorescence emission in the detection band corresponding to the other type of molecule is observed.
- **Poisson distributed quantized emission:** Fluorescence emission is a quantum mechanical process. It is stochastic in nature, and fluorescence emission is quantized. The number of fluorescence photons detected follows a Poisson distribution.
- **Bleaching:** The lifetime of a particle (molecule) capable of converting absorbed light into fluorescence is finite. As the molecule undergoes a number of transitions between excited and ground states, there is a probability for the molecule to dissociate, or to undergo an electronic change (ionization) or a chemical reaction, often resulting in the removal of this fluorophore from the population of available, i.e., emitting, fluorophores in the sample. This “bleaching,” i.e., a loss in fluorescence intensity, is often induced by the illumination of a sample with excitation light, in which case the process is termed *photobleaching*. *Photolysis* is the chemical decomposition of molecules under the influence of light. However, bleaching can also be induced by other means, for example, by embedding fluorophores in a suitable chemical environment. Bleaching is usually discussed in connection with a detection channel. It should be noted that a shift in the emission spectra of a fluorophore (e.g., by protonation or oxygenation) could be confused with bleaching as a similar loss of fluorescence signal is observed in the corresponding detection channel. Likewise, when excitation occurs within a narrow band of wavelengths, a change in the absorption spectra of the fluorophore could have a similar effect. Sometimes, the transition from a fluorescent to a non-fluorescent state is reversible, in which case the terms *transient bleaching* and *reversible bleaching* are occasionally used.
- **Fluorescence lifetime:** The lifetime of the excited (S_1 -)state of a fluorophore is finite. The $1/e$ -decay time of the S_1 -state is characteristic of the type of fluorophore used but is influenced by its nanoenvironment. Typical lifetimes of excited states are in the nanosecond range.

- **Lifetime of triplet state:** A fluorophore might undergo a transition to an electronic triplet (T_1 -)state. This state is typically long-lived (with respect to the fluorescence lifetime) since it involves a transition that is quantum mechanically suppressed. Thus, the fluorophore is no longer available for excitation. However, within a biological sample and at room temperature, relaxation from the triplet state to the ground state is possible, but mostly this does not contribute to the detected fluorescence signal.
- **Lifetime of radical state:** A fluorophore might undergo a reversible transition involving a reduction or oxidation to a radical state from which it might return – after some time – to the non-radical ground state S_0 . The observable effect of this transition on the fluorescence output is very similar to the situation where a fluorophore goes to the triplet state. However, in terms of possible transitions and further chemical reactions, it is not.

Several additional parameters affect detected intensities. A prominent factor is the cross talk between detection channels, which in the case of a color-based separation of detection channels can be attributed to the fact that the wavelengths emitted by a fluorophore light at room temperature are distributed according to the molecular spectrum (vibrational and rotational energy levels), which typically spans across several tens of nanometers, with a tail toward the red end of the spectrum. Therefore, a molecule of a given type might also contribute to a signal detected in another channel, for example, a channel associated to another type of molecule with a peak emission at longer wavelengths. In linear excitation mode, the effect might be corrected to a high degree if the amount of cross talk for any given sample with a selection of fluorophore types and settings for the microscope detection bands is known (e.g., by independent, single-color measurements). In non-linear excitation or stochastic emission mode, this may only be corrected in experiments in which simultaneous registration of all affected detection channels is performed.

1.4.1

Multi-Color Imaging

One of the most difficult aspects of SRM is to perform multi-color experiments. One of the reasons for this is the cross talk discussed earlier. Other reasons are the limited availability of combinations of fluorophores that simultaneously match the imaging conditions of the corresponding SRM technique and the difficulties in multi-color labeling protocols. For all of the present super-resolution techniques, examples of applications of multi-color imaging were demonstrated early in the advent of SRM. Multi-color STED was realized and published already in 2007 [105, 106]. Experiments employing multi-color PALM/STORM were published around the same time [107, 108], as were multi-color experiments using PALM with Independently Running Acquisition (PALMIRA) [109].

Single-molecule localization microscopy employing multiple colors is notoriously difficult if more than two classes of fluorophores are employed. The reasons

for this differ from the constraints imposed by the STED hardware and photostability requirements: Various species of fluorophores react differently to a specific chemical environment dominated by the embedding buffer used for imaging. Consequently, precise control of the blinking behavior of the fluorophores is limited if many classes of fluorophores are mixed, and multi-color images tend to be acquired in sequential mode, with one (or two) color channels recorded at a time, and an in-between exchange of the buffer medium or even exchange of the fluorescent labels. Multi-color applications of SIM and LSFM were proposed early on simply because these linear techniques impose fewer constraints on fluorophores and embedding media.

1.5

Applications to the Study of Nuclear DNA

The human genome has been decoded, but we are still far from understanding the regulation of all gene activities. A largely unexplained role in these regulatory mechanisms is played by the 3D arrangement of genetic material [110]. The visualization and quantitative measurement of the distribution of DNA at high resolution inside the cell nucleus is therefore an essential desideratum in genetics. Current SRM methods offer a 10 nm resolution, allowing in principle to divide a cell with a typical volume of $(10\ \mu\text{m})^3$ into roughly 10^9 super-resolution pixels. If we consider that most eukaryotic cells have around 10^4 genes and that the cellular abundance of each of the transcripts is typically between 10 and 100 copies, the information content that is accessible by SRM is about 1000 times higher than what is needed to encode all of the transcripts within a given cell [111]. Arriving at the goal of a quantitative analysis of the distribution of DNA and of all of the transcripts is a multi-disciplinary endeavor, with collaborative input from molecular and system biologists, polymer physicists, biophysicists, engineers, and computer scientists.

Strong evidence suggests that the genome in mammalian cell nuclei has a highly complex spatial organization (for reviews see, e.g., [110, 112–114]). In addition to the genomic sequence, several other factors are connected to gene activity [115]. For instance, it has been shown that the location [116, 117] and chromatin compaction or condensation [118] of individual genes are correlated to gene activity [119–121]. These factors also influence the accessibility of a given gene locus to macromolecular complexes, for example, to those involved in the process of transcription [122, 123], especially during particular stages [124, 125] or phases of enhanced cell stress [126]. A functionally compartmentalized organization of higher-order chromatin arrangement provides another level of epigenetic gene regulation [19, 127, 128], and it is known from chromosome-conformation-capture studies that topologically associating chromatin domain (TADs) structures are preserved [129–132]. A wealth of molecular and microscopic information has been accumulated, resulting in a variety of – sometimes contradictory – models of nuclear architecture on the nanoscale. For a long time, a major source

of such ambiguities has been constituted by the limits of conventional light microscopy (optical resolution about 200 nm in the object plane/laterally, 600 nm along the optical axis [7]) that made conclusive tests of models on the nanoscale very difficult. The limited resolution in micrographs thus represented a severe setback to a full mechanistic understanding of, for example, transcription/splicing and repair.

Today, commercial super-resolution microscopes are available in the broad field of biomedicine, often in the context of imaging core facilities with a range of microscopy methods available and with highly trained personnel. This is necessary to bridge the gap between microscope “engineers” and microscope “users.” While limitations in microscope optics and resolution have been overcome, challenges remain in the forms of fluorescence labeling and control of fluorescence emission, of sample preparation, and of super-resolution imaging in tissue. To obtain quantitative information on the functional interplay between nuclear structure and nuclear architecture on the one hand and genetic and epigenetic molecular regulatory mechanisms on the other hand, the novel types of microscopes developed in recent years have already shown tremendous potential in the early years of SRM (for a list of applications see, for example, [133]). Studies with the aim of elucidating the functional architecture of the cell nucleus may not only comprise a direct measure of the expression level of gene regions but could also encompass a quantification of the effects of gene regulation, compaction, and epigenetic modifications of a specific gene region on its expression and on the genomic function of spatially neighboring gene regions. At the same time, quantitative predictions could be gained from a joint approach using structural data, as obtained from molecular dynamic simulations of chromatin compaction and folding [134, 135], together with any kind of microscope (light, electron, X-ray microscopy) or with next-generation sequencing (NGS) and other methods in molecular biology.

Today, many computer models allow for the quantitative prediction of the conformation and accessibility of chromatin. In polymer physics, the worm-like chain (WLC) model is often used to describe semi-flexible polymers. Free nucleic acids in solution (e.g., DNA) can be considered a representative of such a polymer, despite the fact that DNA has many properties that are not well described by highly simplified models, and more advanced methods involving, for example, molecular dynamic simulations are used in more sophisticated analyses. However, we will use a simple approximation to the WLC model to illustrate a possible combination of polymer simulations with microscopic analysis.

The WLC model is particularly suited to describe stiffer polymers, in which successive segments display some sort of correlation in terms of their orientation (direction). The quality of this correlation is reflected in the elastic properties of the polymer. For simplicity, in what follows, DNA is considered to be a polymer chain with no torsional stress. Such a chain is often described by the Kratky–Porod model [136] as consisting of N segments of length b and orientation vector $\vec{v}_i = (\sin(\varphi) \sin(\theta), \cos(\varphi) \sin(\theta), \cos(\theta))$ in spherical coordinates. The WLC model is obtained in the limit $b \rightarrow 0$. Figure 1.9 shows the three projections along

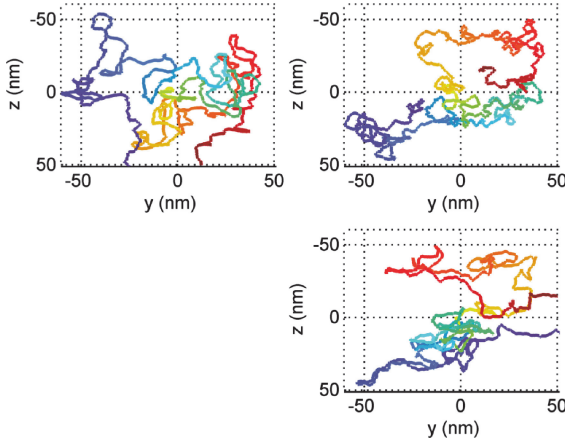


Figure 1.9 Simulation of a polymer using a Kratky–Porod polymer model. A persistence length of ~ 6.1 nm was used in this simulation. In contrast, DNA was found to have a persistence length of ~ 50 nm [137].

(x, y, z) of a simulation of a polymer. Such simulated structures will be used in what follows to illustrate the progress achieved using available advanced light microscopy methods. By means of virtual microscopy (VIM), in which the microscope image is computer-generated based on either the calculated or measured microscope PSF, the true benefit of the respective microscope method when applied to image such a structure can be appreciated.

Figure 1.10 shows z -projections of computer-generated images of the polymer depicted in Figure 1.9 using an assumed resolution of 50 nm. Noise was neglected in the simulation. It is evident that the structure may not be fully resolved. However, additional information may be gained when employing structured illumination, which renders high spatial frequency content accessible in the microscope images: When shifting the phase of the standing wave-field from 0° to

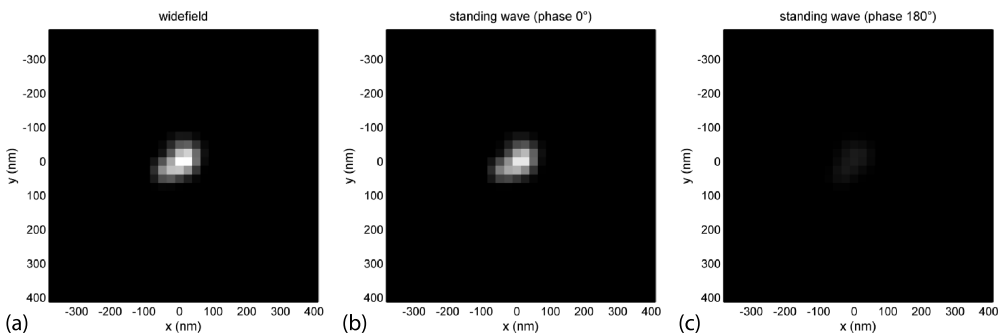


Figure 1.10 Virtual microscopy (VIM) images of a polymer using an assumed resolution of 50 nm in the absence of noise. z -projections are shown for different types of illumination. (a) Wide-field illumination. (b,c) Standing wave illumination along z -axis with 0° and 180° phase angle, respectively, using a 491 nm laser

wavelength. From the relatively low intensities observed in (b) it may be deduced that the structure does not span multiple fringes of the standing wave pattern. This may be used to estimate the upper bound for the size of the labeled polymer structure.

180°, i.e., from high illumination at the origin to zero illumination intensity, the object is only barely visible at severely reduced intensity, indicating that the size of the object is smaller than the modulation wavelength of the standing wave-field, $491 \text{ nm}/(2n) \approx 160 \text{ nm}$. It is also clear that the object has an extent that is in the same range as the values for the resolution limit in optical detection since the image does not resemble a diffraction-limited spot (i.e., it is not round), which means that the object cannot be smaller than $\sim\lambda/10$.

1.6

Other Applications

SRM has been applied to a large range of other biological questions, only a few of which are mentioned here. As discussed earlier, imaging of 3D biological samples has been challenging so far owing to inhomogeneities in their optical properties, resulting in optical aberrations. Optical aberrations generally accumulate with increasing length of the optical path within the sample and with the number of interfaces (membranes) intersecting the optical path. Hence priority in the application of advanced light microscopy (with the exception of LSFM) has been given to imaging surface structures (e.g., receptor proteins [138] and clathrin-coated pits [139]), to imaging inside the cytoplasm (e.g., lysosomes, Golgi apparatus [61, 140]), and to imaging the nuclear envelope or structures constituting parts of this envelope (e.g., nuclear pore complex [76, 141, 142]). Owing to these difficulties, to date, only a few groups have ventured into the realm of super-resolution imaging within the cell nucleus (for a review see [143]). Especially since the introduction of SRM methods in the technology platforms available for medical research, other applications of SRM have been found in the realms of neuroimaging, developmental biology, and cancer research. Another emerging field of application for these imaging methods is cardiovascular research.

References

- 1 Blake, W. and Bloom, H. (2008 [1965]) *The Complete Poetry and Prose of William Blake*, University of California Press, Berkeley, Los Angeles, London, with a New Foreword and Commentary by Harold Bloom.
- 2 Ehrenberg, M. (2014) The Nobel Prize in chemistry 2014 (press release). http://www.nobelprize.org/nobel_prizes/chemistry/laureates/2014/advanced-chemistryprize2014.pdf, scientific Background on the Nobel Prize in Chemistry 2014, published Oct. 8, 2014 by The Royal Swedish Academy of Sciences.
- 3 Tsien, R.Y. (2003) Imagining imaging's future. *Nat. Rev. Mol. Cell Biol.*, **Suppl**, SS16–21.
- 4 Moerner, W.E. and Kador, L. (1989) Optical detection and spectroscopy of single molecules in a solid. *Phys. Rev. Lett.*, **62** (21), 2535. <http://journals.aps.org/prl/abstract/10.1103/PhysRevLett.62.2535>.
- 5 Abbe, E. (1873) Beiträge zur Theorie des Mikroskops und der mikroskopischen Wahrnehmung. *Arch. mikrosk. Anat.*, **9** (1), 413–418. <http://www.springerlink.com/index/k7154700k345404p.pdf>.

- 6 Kubitscheck, U. (2013) *Fluorescence microscopy: From principles to biological applications*, John Wiley & Sons. <http://eu.wiley.com/WileyCDA/WileyTitle/productCd-3527329226.html>, ISBN: 978-3-527-32922-9.
- 7 Born, M. and Wolf, E. (1999) *Principles of Optics*, Cambridge University Press, Cambridge; New York, 7th edn.
- 8 Rayleigh, L. (1896) On the theory of optical images, with special reference to the microscope. *Philos. Mag.*, **42** (255), 167–195. <http://www.tandfonline.com/doi/abs/10.1080/14786449608620902>.
- 9 Babcock, H. and Zhuang, X. (2016) Analyzing Single Molecule Localization Microscopy Data Using Cubic Splines. *bioRxiv*, p. 083402, doi:10.1101/083402.
- 10 Birk, U., Best, G., Amberger, R., and Cremer, C. (2017) Super-Resolution Microscopy: Interference and Pattern Techniques, in *Fluorescence Microscopy: From Principles to Biological Applications*. Wiley-VCH, Weinheim, 2nd edn., pp 291–319.
- 11 Singer, W., Totzeck, M., and Gross, H. (2006) *Handbook of Optical Systems, Physical Image Formation*, John Wiley & Sons.
- 12 Fultz, B. and Howe, J.M. (2007) *Transmission Electron Microscopy and Diffractometry of Materials*, Springer, Heidelberg, 3rd edn. <http://resolver.caltech.edu/CaltechAUTHORS:20121025-210157406>.
- 13 Bogner, A., Jouneau, P.H., Thollet, G., Basset, D., and Gauthier, C. (2007) A history of scanning electron microscopy developments: Towards “wet-STEM” imaging. *Micron*, **38** (4), 390–401, doi:10.1016/j.micron.2006.06.008. <http://linkinghub.elsevier.com/retrieve/pii/S0968432806001016>.
- 14 Knoll, M. and Ruska, E. (1932) Das Elektronenmikroskop. *Z. Phys.*, **78** (5-6), 318–339, doi:10.1007/BF01342199. <http://link.springer.com/article/10.1007/BF01342199>.
- 15 Binnig, G. and Rohrer, H. (1982) Scanning tunneling microscope. US patent #4343993 A. <http://www.google.com/patents/US4343993>.
- 16 Binnig, G., Quate, C.F., and Gerber, C. (1986) Atomic force microscope. *Phys. Rev. Lett.*, **56** (9), 930–933, doi:10.1103/PhysRevLett.56.930. <http://link.aps.org/doi/10.1103/PhysRevLett.56.930>.
- 17 Olins, A.L. and Olins, D.E. Spheroid chromatin units (v bodies), *Science* **183** (4122), 330–332.
- 18 Olins, A.L., Senior, M.B., and Olins, D.E. Ultrastructural features of chromatin nucleosomes, *J. Cell Biol.*, **68** (3), 787–793.
- 19 Rouquette, J., Cremer, C., Cremer, T., and Fakan, S. (2010) Functional nuclear architecture studied by microscopy, in *International Review of Cell and Molecular Biology*, vol. 282, Elsevier, pp. 1–90. <http://linkinghub.elsevier.com/retrieve/pii/S1937644810820015>.
- 20 Ahmed, K., Li, R., and Bazett-Jones, D.P. (2009) Electron spectroscopic imaging of the nuclear landscape. *Methods Mol. Biol.*, **464**, 415–423, doi:10.1007/978-1-60327-461-6_23.
- 21 Cazaux, J. (1995) Correlations between ionization radiation damage and charging effects in transmission electron microscopy. *Ultramicroscopy*, **60** (3), 411–425, doi:10.1016/0304-3991(95)00077-1. <http://www.sciencedirect.com/science/article/pii/0304399195000771>.
- 22 Minsky, M. (1961) Microscopy apparatus. US patent #3 013 467.
- 23 Cremer, C. and Cremer, T. (1978) Considerations on a laser-scanning-microscope with high resolution and depth of field. *Microsc. Acta*, **81** (1), 31–44.
- 24 Brakenhoff, G.J., Blom, P., and Barends, P. (1979) Confocal scanning light microscopy with aperture immersion lenses. *J. Microsc.*, **117**, 219–232.
- 25 Sheppard, C.J.R. and Wilson, T. (1978) Depth of field in the scanning microscope. *Opt. Lett.*, **3** (3), 115–117. <http://www.opticsinfobase.org/abstract.cfm?uri=ol-3-3-115>.
- 26 McCutchen, C.W. (1967) Superresolution in Microscopy and the Abbe Resolution Limit. *J. Opt. Soc. Am.*, **57** (10), 1190–1192, doi:10.1364/JOSA.57.001190.
- 27 Cox, I.J., Sheppard, C.J.R., and Wilson, T. (1982) Super-resolution by confocal

- fluorescent microscopy. *Optik*, **60** (4), 391–396.
- 28 Sheppard, C.J.R. and Wilson, T. (1981) The theory of the direct-view confocal microscope. *J. Microsc.*, **124** (2), 107–117. <http://onlinelibrary.wiley.com/doi/10.1111/j.1365-2818.1981.tb00304.x/abstract>.
 - 29 Masters, B.R. (1996) *Selected Papers on Confocal Microscopy*, SPIE Press, Bellingham, Wash., USA.
 - 30 Muller, M. (2006) *Introduction to Confocal Fluorescence Microscopy*, SPIE Press, ISBN 978-0-8194-6043-1.
 - 31 Stelzer, E.H.K. (1998) Contrast, resolution, pixelation, dynamic range and signal-to-noise ratio: Fundamental limits to resolution in fluorescence light microscopy. *J. Microsc.*, **189** (1), 15–24, doi:10.1046/j.1365-2818.1998.00290.x.
 - 32 Dittrich, P.S. and Schwille, P. (2014) Photobleaching and stabilization of fluorophores used for single-molecule analysis with one- and two-photon excitation. *Appl. Phys. B*, **73** (8), 829–837, doi:10.1007/s003400100737. <http://link.springer.com/article/10.1007/s003400100737>.
 - 33 Eggeling, C., Widengren, J., Rigler, R., and Seidel, C.A.M. (1998) Photobleaching of fluorescent dyes under conditions used for single-molecule detection: Evidence of two-step photolysis. *Anal. Chem.*, **70** (13), 2651–2659, doi:10.1021/ac980027p. <http://dx.doi.org/10.1021/ac980027p>.
 - 34 Widengren, J. and Rigler, R. (1996) Mechanisms of photobleaching investigated by fluorescence correlation spectroscopy. *Bioimaging*, **4** (3), 149–157, doi:10.1002/1361-6374(199609)4:3<149::AID-BIO5>3.0.CO;2-D. [http://onlinelibrary.wiley.com/doi/10.1002/1361-6374\(199609\)4:3<149::AID-BIO5>3.0.CO;2-D/abstract](http://onlinelibrary.wiley.com/doi/10.1002/1361-6374(199609)4:3<149::AID-BIO5>3.0.CO;2-D/abstract).
 - 35 Denk, W., Strickler, J.H., and Webb, W.W. (1990) 2-photon laser scanning fluorescence microscopy. *Science*, **248**, 73–76.
 - 36 Brakenhoff, G.J., Squier, J., Norris, T., Bliton, A.C., Wade, M.H., and Athey, B. (1996) Real-time two-photon confocal microscopy using a femtosecond, amplified Ti:sapphire system. *J. Microsc.*, **181** (Pt 3), 253–259.
 - 37 Bewersdorf, J., Pick, R., and Hell, S.W. (1998) Multifocal multiphoton microscopy. *Opt. Lett.*, **23**, 655–657.
 - 38 Oron, D., Tal, E., and Silberberg, Y. (2005) Scanningless depth-resolved microscopy. *Opt. Express*, **13** (5), 1468–1476, doi:10.1364/OPEX.13.001468. <http://www.osapublishing.org/abstract.cfm?uri=oe-13-5-1468>.
 - 39 Frey, H.G., Bolwien, C., Brandenburg, A., Ros, R., and Anselmetti, D. (2006) Optimized apertureless optical near-field probes with 15 nm optical resolution. *Nanotechnology*, **17** (13), 3105, doi:10.1088/0957-4484/17/13/004. <http://iopscience.iop.org/0957-4484/17/13/004>.
 - 40 Bortchagovsky, E., Francs, G.C.d., Molenda, D., Naber, A., and Fischer, U.C. (2006) Transmission of an obliquely incident beam of light through small apertures in a metal film. *Appl. Phys. B*, **84** (1/2), 49–53, doi:10.1007/s00340-006-2296-9. <http://link.springer.com/article/10.1007/s00340-006-2296-9>.
 - 41 Dunn, R.C. (1999) Near-field scanning optical microscopy. *Chem. Rev.*, **99** (10), 2891–2928.
 - 42 Pohl, D.W., Denk, W., and Lanz, M. (1984) Optical stethoscopy: Image recording with resolution $\lambda/20$. *Appl. Phys. Lett.*, **44**, 651–653, doi:10.1063/1.94865. <http://adsabs.harvard.edu/abs/1984ApPhL..44..651P>.
 - 43 Lewis, A., Isaacson, M., Harootunian, A., and Muray, A. (1984) Development of a 500 Å spatial resolution light microscope. *Ultramicroscopy*, **13** (3), 227–231, doi:10.1016/0304-3991(84)90201-8. [http://dx.doi.org/10.1016/0304-3991\(84\)90201-8](http://dx.doi.org/10.1016/0304-3991(84)90201-8).
 - 44 Betzig, E., Lewis, A., Harootunian, A., Isaacson, M., and Kratschmer, E. (1986) Near field scanning optical microscopy (NSOM): Development and biophysical applications. *Biophys. J.*, **49** (1), 269–279, doi:10.1016/S0006-3495(86)83640-2. <http://www.sciencedirect.com/science/article/pii/S0006349586836402>.
 - 45 Toraldo di Francia, G. (1955) Resolving power and information. *J. Opt. Soc. Am.*, **45** (7), 497–499, doi:10.1364/JOSA.45.000497. <http://www.opticsinfobase.org/abstract.cfm?URI=josa-45-7-497>.

- 46 Wagner, C., Hildenbrand, G., Spöri, U., and Cremer, C. (2006) Beyond nanosizing: An approach to shape analysis of fluorescent nanostructures by SMI-microscopy. *Optik*, **117** (1), 26–32, doi:10.1016/j.jjleo.2005.05.006. <http://www.sciencedirect.com/science/article/pii/S0030402605001300>.
- 47 Baddeley, D., Weiland, Y., Batram, C., Birk, U., and Cremer, C. (2010) Model based precision structural measurements on barely resolved objects. *J. Microsc.*, **237** (1), 70–78, doi:10.1111/j.1365-2818.2009.03304.x. <http://www.ncbi.nlm.nih.gov/pubmed/20055920>.
- 48 Cox, S., Rosten, E., Monypenny, J., Jovanovic-Taliman, T., Burnette, D.T., Lippincott-Schwartz, J., Jones, G.E., and Heintzmann, R. (2012) Bayesian localization microscopy reveals nanoscale podosome dynamics. *Nat. Methods*, **9** (2), 195–200, doi:10.1038/nmeth.1812. <http://www.nature.com/nmeth/journal/v9/n2/full/nmeth.1812.html>.
- 49 Betzig, E. (1995) Proposed method for molecular optical imaging. *Opt. Lett.*, **20** (3), 237–239. <http://www.opticsinfobase.org/abstract.cfm?id=34075>.
- 50 Cremer, C. and Cremer, T. (1972) Verfahren zur Darstellung bzw. Modifikation von Objekt-Details, deren Abmessungen außerhalb der sichtbaren Wellenlängen liegen. DE patent #2116521.
- 51 Hell, S. and Stelzer, E.H. (1992) Fundamental improvement of resolution with a 4Pi-confocal fluorescence microscope using two-photon excitation. *Opt. Commun.*, **93** (5), 277–282. <http://www.sciencedirect.com/science/article/pii/003040189290185T>.
- 52 Lanni, F. (1986) Standing-wave fluorescence microscopy, in *Applications of Fluorescence in the Biomedical Sciences* (eds D.L. Taylor, A.S. Waggoner, R.F. Murphy, F. Lanni, and R.R. Birge), A. R. Liss. Inc., New York, pp. 505–521.
- 53 Bailey, B., Farkas, D.L., Taylor, D.L., and Lanni, F. (1993) Enhancement of axial resolution in fluorescence microscopy by standing-wave excitation. *Nature*, **366**, 44–48.
- 54 Gustafsson, M.G.L., Agard, D.A., and Sedat, J.W. (1996) 3D widefield microscopy with two objective lenses: Experimental verification of improved axial resolution. *Proc. SPIE*, **2655**, 62.
- 55 Gustafsson, M.G., Agard, D.A., and Sedat, J.W. (1999) I5M: 3D widefield light microscopy with better than 100 nm axial resolution. *J. Microsc.*, **195** (Pt 1), 10–16.
- 56 Hell, S.W., Lindek, S., Cremer, C., and Stelzer, E.H.K. (1994) Measurement of 4Pi-confocal point spread function proves 75 nm axial resolution. *Appl. Phys. Lett.*, **64** (11), 1335–1337.
- 57 Heintzmann, R. and Cremer, C.G. (1999) Laterally modulated excitation microscopy: Improvement of resolution by using a diffraction grating, in *SPIE BiOS Europe'98*, pp. 185–196. <http://proceedings.spiedigitallibrary.org/proceeding.aspx?articleid=972650>.
- 58 Gustafsson, M.G. (2000) Surpassing the lateral resolution limit by a factor of two using structured illumination microscopy. *J. Microsc.*, **198** (2), 82–87. <http://onlinelibrary.wiley.com/doi/10.1046/j.1365-2818.2000.00710.x/full>.
- 59 Mathée, H., Baddeley, D., Wotzlaw, C., Cremer, C., and Birk, U. (2007) Spatially modulated illumination microscopy using one objective lens. *Opt. Eng.*, **46**, 083603.
- 60 Lanni, F., Waggoner, A.S., and Taylor, D.L. (1986) Standing-wave luminescence microscopy. US patent #4 621 911.
- 61 Betzig, E., Patterson, G.H., Sougrat, R., Lindwasser, O.W., Olenych, S., Bonifacino, J.S., Davidson, M.W., Lippincott-Schwartz, J., and Hess, H.F. (2006) Imaging intracellular fluorescent proteins at nanometer resolution. *Science*, **313** (5793), 1642–1645, doi:10.1126/science.1127344.
- 62 Rust, M.J., Bates, M., and Zhuang, X. (2006) Sub-diffraction-limit imaging by stochastic optical reconstruction microscopy (STORM). *Nat. Methods*, **3** (10), 793–796. <http://www.nature.com/nmeth/journal/vaop/ncurrent/full/nmeth929.html>.

- 63 Fujita, K., Kobayashi, M., Kawano, S., Yamanaka, M., and Kawata, S. (2007) High-resolution confocal microscopy by saturated excitation of fluorescence. *Phys. Rev. Lett.*, **99** (22), 228105, doi:10.1103/PhysRevLett.99.228105. <http://link.aps.org/doi/10.1103/PhysRevLett.99.228105>.
- 64 Heintzmann, R., Jovin, T.M., and Cremer, C. (2002) Saturated patterned excitation microscopy – A concept for optical resolution improvement. *J. Opt. Soc. Am. A*, **19** (8), 1599–1609, doi:10.1364/JOSAA.19.001599.
- 65 Gustafsson, M.G. (2005) Nonlinear structured-illumination microscopy: Wide-field fluorescence imaging with theoretically unlimited resolution. *Proc. Natl. Acad. Sci. USA*, **102** (37), 13081–13086.
- 66 Hell, S.W. and Wichmann, J. (1994) Breaking the diffraction resolution limit by stimulated emission: Stimulated-emission-depletion fluorescence microscopy. *Opt. Lett.*, **19**, 780–782.
- 67 Fölling, J., Bossi, M., Bock, H., Medda, R., Wurm, C.A., Hein, B., Jakobs, S., Eggeling, C., and Hell, S.W. (2008) Fluorescence nanoscopy by ground-state depletion and single-molecule return. *Nat. Methods*, **5** (11), 943–945. <http://www.nature.com/nmeth/journal/vaop/ncurrent/full/nmeth.1257.html>.
- 68 Hess, S.T., Girirajan, T.P., and Mason, M.D. (2006) Ultra-high resolution imaging by fluorescence photoactivation localization microscopy. *Biophys. J.*, **91** (11), 4258–4272. <http://www.ncbi.nlm.nih.gov/pmc/articles/PMC1635685/>.
- 69 Schoen, I., Ries, J., Klotzsch, E., Ewers, H., and Vogel, V. (2011) Binding-activated localization microscopy of DNA structures. *Nano Lett.*, **11** (9), 4008–4011, doi:10.1021/nl2025954. <http://pubs.acs.org/doi/abs/10.1021/nl2025954>.
- 70 Gordon, M.P., Ha, T., and Selvin, P.R. (2004) Single-molecule high-resolution imaging with photobleaching. *Proc. Natl. Acad. Sci. USA*, **101** (17), 6462–6465, doi:10.1073/pnas.0401638101. <http://www.pnas.org/content/101/17/6462>.
- 71 Qu, X., Wu, D., Mets, L., and Scherer, N.F. (2004) Nanometer-localized multiple single-molecule fluorescence microscopy. *Proc. Natl. Acad. Sci. USA*, **101** (31), 11298–11303, doi:10.1073/pnas.0402155101. <http://www.pnas.org/content/101/31/11298>.
- 72 Heilemann, M., van de Linde, S., Schüttelpelz, M., Kasper, R., Seefeldt, B., Mukherjee, A., Tinnefeld, P., and Sauer, M. (2008) Subdiffraction-resolution fluorescence imaging with conventional fluorescent probes. *Angew. Chem. Int. Ed.*, **47** (33), 6172–6176. <http://onlinelibrary.wiley.com/doi/10.1002/anie.200802376/full>.
- 73 Lemmer, P., Gunkel, M., Baddeley, D., Kaufmann, R., Urich, A., Weiland, Y., Reymann, J., Müller, P., Hausmann, M., and Cremer, C. (2008) SPDM: Light microscopy with single-molecule resolution at the nanoscale. *Appl. Phys. B*, **93** (1), 1–12. <http://link.springer.com/article/10.1007/s00340-008-3152-x>.
- 74 Burnette, D.T., Sengupta, P., Dai, Y., Lippincott-Schwartz, J., and Kachar, B. (2011) Bleaching/blinking assisted localization microscopy for superresolution imaging using standard fluorescent molecules. *Proc. Natl. Acad. Sci. USA*, **108** (52), 21081–21086, doi:10.1073/pnas.1117430109.
- 75 Simonson, P.D., Rothenberg, E., and Selvin, P.R. (2011) Single-molecule-based super-resolution images in the presence of multiple fluorophores. *Nano Lett.*, **11** (11), 5090–5096, doi:10.1021/nl203560r.
- 76 Reymann, J., Baddeley, D., Gunkel, M., Lemmer, P., Stadter, W., Jegou, T., Rippe, K., Cremer, C., and Birk, U. (2008) High-precision structural analysis of subnuclear complexes in fixed and live cells via spatially modulated illumination (SMI) microscopy. *Chromosome Res.*, **16** (3), 367–382, doi:10.1007/s10577-008-1238-2.
- 77 Lang, M., Müller, T., Engelhardt, J., and Hell, S.W. (2007) 4Pi microscopy of type A with 1-photon excitation in biological fluorescence imaging. *Opt. Express*, **15** (5), 2459, doi:10.1364/OE.15.002459.
- 78 Lang, M.C., Engelhardt, J., and Hell, S.W. (2007) 4Pi microscopy with lin-

- ear fluorescence excitation. *Opt. Lett.*, **32** (3), 259–261.
- 79 Lang, M.C., Staudt, T., Engelhardt, J., and Hell, S.W. (2008) 4Pi microscopy with negligible sidelobes. *New J. Phys.*, **10** (4), 043041, doi:10.1088/1367-2630/10/4/043041.
- 80 Hell, S.W. (2010) Far-field optical nanoscopy, in *Single Molecule Spectroscopy in Chemistry, Physics and Biology* (eds A. Gräslund, R. Rigler, and J. Widengren), Springer, pp. 365–398.
- 81 Spöri, U., Failla, A.V., and Cremer, C. (2004) Superresolution size determination in fluorescence microscopy: A comparison between spatially modulated illumination and confocal laser scanning microscopy. *J. Appl. Phys.*, **95** (12), 8436–43.
- 82 Rossberger, S., Best, G., Baddeley, D., Heintzmann, R., Birk, U., Dithmar, S., and Cremer, C. (2013) Combination of structured illumination and single molecule localization microscopy in one setup. *J. Opt.*, **15** (9), 094003. <http://iopscience.iop.org/2040-8986/15/9/094003>.
- 83 Wagner, C., Spöri, U., and Cremer, C. (2005) High-precision SMI microscopy size measurements by simultaneous frequency domain reconstruction of the axial point spread function. *Optik*, **116** (1), 15–21.
- 84 Hemmer, P.R. and Zapata, T. (2012) The universal scaling laws that determine the achievable resolution in different schemes for super-resolution imaging. *J. Opt.*, **14** (8), 083002, doi:10.1088/2040-8978/14/8/083002.
- 85 Patterson, G.H. and Lippincott-Schwartz, J. (2002) A photoactivatable GFP for selective photolabeling of proteins and cells. *Science*, **297** (5588), 1873–1877, doi:10.1126/science.1074952.
- 86 Chudakov, D.M., Belousov, V.V., Zraisky, A.G., Novoselov, V.V., Staroverov, D.B., Zorov, D.B., Lukyanov, S., and Lukyanov, K.A. (2003) Kindling fluorescent proteins for precise in vivo photolabeling. *Nat. Biotechnol.*, **21** (2), 191–194, doi:10.1038/nbt778.
- 87 Ando, R., Mizuno, H., and Miyawaki, A. (2004) Regulated fast nucleocytoplasmic shuttling observed by reversible protein highlighting. *Science*, **306** (5700), 1370–1373, doi:10.1126/science.1102506.
- 88 Chudakov, D.M., Verkhusha, V.V., Staroverov, D.B., Souslova, E.A., Lukyanov, S., and Lukyanov, K.A. (2004) Photoswitchable cyan fluorescent protein for protein tracking. *Nat. Biotechnol.*, **22** (11), 1435–1439, doi:10.1038/nbt1025.
- 89 Rego, E.H., Shao, L., Macklin, J.J., Winto, L., Johansson, G.A., Kamps-Hughes, N., Davidson, M.W., and Gustafsson, M.G.L. (2012) Nonlinear structured-illumination microscopy with a photoswitchable protein reveals cellular structures at 50 nm resolution. *Proc. Natl. Acad. Sci. USA*, **109** (3), E135–E143, doi:10.1073/pnas.1107547108.
- 90 Dertinger, T., Colyer, R., Iyer, G., Weiss, S., and Enderlein, J. (2009) Fast, background-free, 3D super-resolution optical fluctuation imaging (SOFI). *Proc. Natl. Acad. Sci. USA*, **106** (52), 22287–22292, doi:10.1073/pnas.0907866106. <http://www.ncbi.nlm.nih.gov/pmc/articles/PMC2799731/>.
- 91 Klar, T.A., Jakobs, S., Dyba, M., Egner, A., and Hell, S.W. (2000) Fluorescence microscopy with diffraction resolution barrier broken by stimulated emission. *Proc. Natl. Acad. Sci. USA*, **97**, 8206–8210.
- 92 Osseforth, C., Moffitt, J.R., Schermelleh, L., and Michaelis, J. (2014) Simultaneous dual-color 3D STED microscopy. *Opt. Express*, **22** (6), 7028, doi:10.1364/OE.22.007028. <http://www.opticsinfobase.org/abstract.cfm?URI=oe-22-6-7028>.
- 93 Bornfleth, H., Saetzler, K., Eils, R., and Cremer, C. (1998) High-precision distance measurements and volume-conserving segmentation of objects near and below the resolution limit in three-dimensional confocal fluorescence microscopy. *J. Microsc.*, **189** (2), 118–136. <http://onlinelibrary.wiley.com/doi/10.1046/j.1365-2818.1998.00276.x/full>.
- 94 Esa, A., Edelman, P., Kreth, G., Trakhtenbrot, L., Amariglio, N., Rechavi, G., Hausmann, M., and Cremer, C. (2000) Three-dimensional spectral pre-

- cision distance microscopy of chromatin nanostructures after triple-colour DNA labelling: A study of the BCR region on chromosome 22 and the Philadelphia chromosome. *J. Microsc.*, **199** (Pt 2), 96–105.
- 95 Esa, A., Trakhtenbrot, L., Hausmann, M., Rauch, J., Brok-Simoni, F., Rechavi, G., Ben-Bassat, I., and Cremer, C. (1998) Fast-FISH detection and semi-automated image analysis of numerical chromosome aberrations in hematological malignancies. *Anal. Cell Pathol.*, **16** (4), 211–222.
- 96 Lacoste, T.D., Michalet, X., Pinaud, F., Chemla, D.S., Alivisatos, A.P., and Weiss, S. (2000) Ultrahigh-resolution multicolor colocalization of single fluorescent probes. *Proc. Natl. Acad. Sci. USA*, **97** (17), 9461–9466.
- 97 Van Oijen, A.M., Köhler, J., Schmidt, J., Müller, M., and Brakenhoff, G.J. (1998) 3-dimensional super-resolution by spectrally selective imaging. *Chem. Phys. Lett.*, **292** (1), 183–187. <http://www.sciencedirect.com/science/article/pii/S0009261498006733>.
- 98 Edelmann, P., Esa, A., Hausmann, M., and Cremer, C. (1999) Confocal laser-scanning microscopy: In situ determination of the confocal point-spread function and the chromatic shifts in intact cell nuclei. *Optik*, **110** (4), 194–198.
- 99 Cremer, C., Edelmann, P., Bornfleth, H., Kreth, G., Muench, H., Luz, H., and Hausmann, M. (1999) Principles of spectral precision distance confocal microscopy for the analysis of molecular nuclear structure, in *Handbook of Computer Vision and Applications*, vol. 3 Systems and Applications (eds B. Jähne, H. Haussecker, and P. Geißler), Academic Press, San Diego, London, pp. 839–857, 1st edn.
- 100 Speicher, M.R., Ballard, S.G., and Ward, D.C. (1996) Karyotyping human chromosomes by combinatorial multi-fluor FISH. *Nat. Genet.*, **12**, 368–375.
- 101 Lakowicz, J.R., Szmazinski, H., and Nowaczyk, K. (1992) Fluorescence lifetime imaging. *Proc. Natl. Acad. Sci. USA*, **89**, 1271–1275.
- 102 Schoenle, A., Glatz, M., and Hell, S.W. (2000) Four-dimensional multiphoton microscopy with time-correlated single-photon counting. *Appl. Opt.*, **39**, 6306–6311.
- 103 Heilemann, M., Herten, D.P., Heintzmann, R., Cremer, C., Müller, C., Tinnefeld, P., Weston, K.D., Wolfrum, J., and Sauer, M. (2002) High-resolution colocalization of single dye molecules by fluorescence lifetime imaging microscopy. *Anal. Chem.*, **74** (14), 3511–3517, doi:10.1021/ac025576g. <http://pubs.acs.org/doi/abs/10.1021/ac025576g>.
- 104 Sauer, M., Hofkens, J., and Enderlein, J. (2011) *Handbook of fluorescence spectroscopy and imaging: From single molecules to ensembles*, Wiley-VCH Verlag GmbH, Weinheim.
- 105 Donnert, G., Keller, J., Wurm, C.A., Rizzoli, S.O., Westphal, V., Schönle, A., Jahn, R., Jakobs, S., Eggeling, C., and Hell, S.W. (2007) Two-color far-field fluorescence nanoscopy. *Biophys. J.*, **92** (8), L67–L69, doi:10.1529/biophysj.107.104497.
- 106 Schmidt, R., Wurm, C.A., Jakobs, S., Engelhardt, J., Egner, A., and Hell, S.W. (2008) Spherical nanosized focal spot unravels the interior of cells. *Nat. Methods*, **5** (6), 539–544, doi:10.1038/nmeth.1214. <http://www.nature.com/nmeth/journal/v5/n6/full/nmeth.1214.html>.
- 107 Bates, M., Huang, B., Dempsey, G.T., and Zhuang, X. (2007) Multicolor super-resolution imaging with photo-switchable fluorescent probes. *Science*, **317** (5845), 1749–1753, doi:10.1126/science.1146598. <http://www.sciencemag.org/content/317/5845/1749>.
- 108 Bossi, M., Fölling, J., Belov, V.N., Boyarskiy, V.P., Medda, R., Egner, A., Eggeling, C., Schönle, A., and Hell, S.W. (2008) Multicolor far-field fluorescence nanoscopy through isolated detection of distinct molecular species. *Nano Lett.*, **8** (8), 2463–2468, doi:10.1021/nl801471d. <http://dx.doi.org/10.1021/nl801471d>.
- 109 Bock, H., Geisler, C., Wurm, C.A., Von Middendorff, C., Jakobs, S., Schönle, A., Egner, A., Hell, S.W., and Eggeling, C. (2007) Two-color far-field fluorescence nanoscopy based on photoswitch-

- able emitters. *Appl. Phys. B*, **88** (2), 161–165. <http://link.springer.com/article/10.1007/s00340-007-2729-0>.
- 110 Cremer, T., Cremer, M., Hübner, B., Strickfaden, H., Smeets, D., Popken, J., Sterr, M., Markaki, Y., Rippe, K., and Cremer, C. (2015) The 4D nucleome: Evidence for a dynamic nuclear landscape based on co-aligned active and inactive nuclear compartments. *FEBS Letters*, **0** (0), doi:10.1016/j.febslet.2015.05.037. <http://www.febsletters.org/article/S0014579315004317/abstract>.
- 111 Cai, L. (2013) Turning single cells into microarrays by super-resolution barcoding. *Briefings in functional genomics*, **12** (2), 75–80, doi:10.1093/bfgp/els054. <http://www.ncbi.nlm.nih.gov/pmc/articles/PMC3609437/>.
- 112 Fraser, J., Williamson, I., Bickmore, W.A., and Dostie, J. (2015) An Overview of Genome Organization and How We Got There: From FISH to Hi-C. **79** (3), 347–372. doi: 10.1128/MMBR.00006-15.
- 113 van den Heuvel, A., Stadhouders, R., Andrieu-Soler, C., Grosveld, F., and Soler, E. Long-range gene regulation and novel therapeutic applications. **125** (10), 1521–1525. doi: 10.1182/blood-2014-11-567925.
- 114 Chow, J.C. and Heard, E. (2010) Nuclear organization and dosage compensation. **2** (11), a000604, doi: 10.1101/cshperspect.a000604.
- 115 Jaenisch, R. and Bird, A. (2003) Epigenetic regulation of gene expression: How the genome integrates intrinsic and environmental signals. *Nat. Genet.*, **33**, 245–254, doi:10.1038/ng1089. <http://www.nature.com/ng/journal/v33/n3s/full/ng1089.html>.
- 116 Bartova, E., Kozubek, S., Jirsova, P., Kozubek, M., Gajova, H., Lukasova, E., Skalnikova, M., Ganova, A., Koutna, I., and Hausmann, M. (2002) Nuclear topography and gene activity in human differentiated cells. *J. Struct. Biol.*, **139**, 76–89.
- 117 Cremer, T. and Cremer, C. (2001) Chromosome territories, nuclear architecture and gene regulation in mammalian cells. *Nat. Rev. Genet.*, **2** (4), 292–301, doi:10.1038/35066075. http://www.nature.com/nrg/journal/v2/n4/full/nrg0401_292a.html.
- 118 Chambeyron, S. and Bickmore, W.A. (2004) Chromatin decondensation and nuclear reorganization of the HoxB locus upon induction of transcription. *Genes Dev.*, **18** (10), 1119–1130.
- 119 Hildenbrand, G., Rapp, A., Spöri, U., Wagner, C., Cremer, C., and Hausmann, M. (2005) Nano-sizing of specific gene domains in intact human cell nuclei by spatially modulated illumination light microscopy. *Biophys. J.*, **88** (6), 4312–4318, doi:10.1529/biophysj.104.056796. <http://www.sciencedirect.com/science/article/pii/S0006349505734809>.
- 120 Mathée, H., Baddeley, D., Wotzlaw, C., Fandrey, J., Cremer, C., and Birk, U. (2006) Nanostructure of specific chromatin regions and nuclear complexes. *Histochem. Cell Biol.*, **125** (1-2), 75–82, doi:10.1007/s00418-005-0096-7. <http://link.springer.com/article/10.1007/s00418-005-0096-7>.
- 121 Birk, U.J., Baddeley, D., and Cremer, C. (2009) Nanosizing by spatially modulated illumination (SMI) microscopy and applications to the nucleus, in *The Nucleus, Methods in Molecular Biology*, vol. 2 (ed. R. Hancock), Springer, Berlin, Heidelberg, New York, pp. 389–402.
- 122 Spector, D.L. (2003) The dynamics of chromosome organization and gene regulation. *Annu. Rev. Biochem.*, **72** (1), 573–608, doi:10.1146/annurev.biochem.72.121801.161724. <http://dx.doi.org/10.1146/annurev.biochem.72.121801.161724>.
- 123 van Driel, R., Fransz, P.F., and Verschure, P.J. (2003) The eukaryotic genome: A system regulated at different hierarchical levels. *J. Cell Sci.*, **116** (Pt 20), 4067–4075.
- 124 Prakash, K., Fournier, D., Redl, S., Best, G., Borsos, M., Tiwari, V.K., Tachibana-Konwalski, K., Ketting, R.F., Parekh, S.H., Cremer, C., and others (2015) Superresolution imaging reveals structurally distinct periodic patterns of chromatin along pachytene chromosomes. *Proceedings of the National Academy of Sciences*, **112** (47), 14 635–14 640, doi:10.1073/pnas.1516928112.

- 125 Żurek-Biesiada, D., Szczurek, A.T., Prakash, K., Mohana, G.K., Lee, H.K., Roignant, J.Y., Birk, U., Dobrucki, J.W., and Cremer, C. (2015) Localization microscopy of DNA in situ using Vybrant® DyeCycle™ Violet fluorescent probe: A new approach to study nuclear nanostructure at single molecule resolution. *Exp. Cell Res.*, doi:10.1016/j.yexcr.2015.08.020.
- 126 Kirmes, I., Szczurek, A., Prakash, K., Charapitsa, I., Heiser, C., Musheev, M., Schock, F., Fornalczyk, K., Ma, D., Birk, U., Cremer, C., and Reid, G. (2015) A transient ischemic environment induces reversible compaction of chromatin. *Genome Biol.*, **16** (1), 246, doi:10.1186/s13059-015-0802-2.
- 127 Levesque, M.J. and Raj, A. (2013) Single-chromosome transcriptional profiling reveals chromosomal gene expression regulation. *Nat. Methods*, **10** (3), 246–248, doi:10.1038/nmeth.2372. <http://www.nature.com/nmeth/journal/v10/n3/full/nmeth.2372.html>.
- 128 Smeets, D., Markaki, Y., Schmid, V.J., Kraus, F., Tattermusch, A., Cerase, A., Sterr, M., Fiedler, S., Demmerle, J., Popken, J., Leonhardt, H., Brockdorff, N., Cremer, T., Schermelleh, L., and Cremer, M. (2014) Three-dimensional super-resolution microscopy of the inactive X chromosome territory reveals a collapse of its active nuclear compartment harboring distinct Xist RNA foci. *Epigenet. Chromatin*, **7** (1), 8, doi:10.1186/1756-8935-7-8. <http://www.epigeneticsandchromatin.com/content/7/1/8/abstract>.
- 129 Dixon, J.R., Selvaraj, S., Yue, F., Kim, A., Li, Y., Shen, Y., Hu, M., Liu, J.S., and Ren, B. (2012) Topological domains in mammalian genomes identified by analysis of chromatin interactions. *Nature*, **485** (7398), 376–380, doi:10.1038/nature11082.
- 130 Nora, E.P., Lajoie, B.R., Schulz, E.G., Giorgetti, L., Okamoto, I., Servant, N., Piolot, T., van Berkum, N.L., Meisig, J., Sedat, J., Gribnau, J., Barillot, E., Blüthgen, N., Dekker, J., and Heard, E. (2012) Spatial partitioning of the regulatory landscape of the X-inactivation centre. *Nature*, **485** (7398), 381–385, doi:10.1038/nature11049.
- 131 Sexton, T., Yaffe, E., Kenigsberg, E., Bantignies, F., Leblanc, B., Hoichman, M., Parrinello, H., Tanay, A., and Cavalieri, G. (2012) Three-dimensional folding and functional organization principles of the Drosophila genome. *Cell*, **148** (3), 458–472, doi:10.1016/j.cell.2012.01.010.
- 132 Hou, C., Li, L., Qin, Z.S., and Corces, V.G. (2012) Gene density, transcription, and insulators contribute to the partition of the Drosophila genome into physical domains. *Molecular Cell*, **48** (3), 471–484, doi:10.1016/j.molcel.2012.08.031.
- 133 Birk, U.J. and Hausmann, M. (2009) Festschrift to recognise and celebrate Christoph Cremer's contribution to the field of biophysics on the occasion of his 65th birthday. *Eur. Biophys. J.*, **38** (6), 719–720.
- 134 Odenheimer, J., Kreth, G., and Heermann, D.W. (2005) Dynamic simulation of active/inactive chromatin domains. *J. Biol. Phys.*, **31** (3/4), 351–363.
- 135 Diesinger, P.M. and Heermann, D.W. (2010) Monte Carlo simulations indicate that chromatin: Nanostructure is accessible by light microscopy. *BMC Biophys.*, **3** (1), 11. <http://www.biomedcentral.com/1757-5036/3/11>.
- 136 Kratky, O. and Porod, G. (1949) Diffuse small-angle scattering of X-rays in colloid systems. *J. Colloid Sci.*, **4** (1), 35–70, doi:10.1016/0095-8522(49)90032-X. <http://www.sciencedirect.com/science/article/pii/009585224990032X>.
- 137 Langowski, J. and Heermann, D.W. (2007) Computational modeling of the chromatin fiber. *Semin. Cell Dev. Biol.*, **18** (5), 659–667, doi:10.1016/j.semdb.2007.08.011.
- 138 Birk, U.J., Upmann, I., Toomre, D., Wagner, C., and Cremer, C. (2007) Size estimation of protein clusters in the nanometer range by using spatially modulated illumination microscopy, in *Modern Research and Educational Topics in Microscopy, Microscopy Series 3*, vol. 1 (eds A. Mendez-Vilas and J. Diaz), Formatex, Badajoz, Spain, pp. 272–279.

- 139 Huang, B., Wang, W., Bates, M., and Zhuang, X. (2008) Three-dimensional super-resolution imaging by stochastic optical reconstruction microscopy. *Science*, **319** (5864), 810–813. doi:10.1126/science.1153529. <http://www.ncbi.nlm.nih.gov/pmc/articles/PMC2633023/>.
- 140 Egner, A., Verrier, S., Goroshkov, A., Soling, H.D., and Hell, S.W. (2004) 4Pi-microscopy of the Golgi apparatus in live mammalian cells. *J. Struct. Biol.*, **147** (1), 70–76.
- 141 Szyborska, A., Marco, A.d., Daigle, N., Cordes, V.C., Briggs, J.A.G., and Ellenberg, J. (2013) Nuclear pore scaffold structure analyzed by super-resolution microscopy and particle averaging. *Science*, **341** (6146), 655–658. doi:10.1126/science.1240672. <http://www.sciencemag.org/content/341/6146/655>.
- 142 Löscherger, A., van de Linde, S., Dabauvalle, M.C., Rieger, B., Heilemann, M., Krohne, G., and Sauer, M. (2012) Super-resolution imaging visualizes the eightfold symmetry of gp210 proteins around the nuclear pore complex and resolves the central channel with nanometer resolution. *J. Cell Sci.*, **125** (3), 570–575. <http://jcs.biologists.org/content/125/3/570.short>.
- 143 Herbert, S., Soares, H., Zimmer, C., and Henriques, R. (2012) Single-molecule localization super-resolution microscopy: Deeper and faster. *Microw. Microanal.*, **18** (06), 1419–1429. doi:10.1017/S1431927612013347. http://www.journals.cambridge.org/abstract_S1431927612013347.

